# Deep Eutectic Solvents for Electrochemical Energy Storage and Conversion: Progress, Challenges, and Perspectives

## Abstract

The pursuit of efficient green energy utilization arouses increasing interest in producing durable battery materials and catalysts with minimum environmental impact. Deep eutectic solvents (DESs), as green, safe, and cheap analogues of ionic liquids, are emerging candidates for applications including, but not limited to, electrochemical energy storage and conversion. Herein, fundamental investigation of DESs, along with their energy storage and catalytic applications, are reviewed. The important roles that DESs play in various energy storage and conversion technologies are highlighted, such as advanced electrolytes for batteries/supercapacitors, media for the synthesis of electrode materials and catalysts, as well as extracting agents for battery recycling. Finally, the challenges for the controllable synthesis of DESs and applications are proposed, and the potential research directions are delineated. DESs provide tremendous opportunities and open up attractive perspectives as charge transfer and reaction media for energy related applications. It is expected that this review could offer guidance for the future design of advanced DESs towards next-generation energy storage and conversion systems.

**Keywords**: Deep eutectic solvents, energy storage and conversion, advanced electrolytes, functional nanomaterials, battery recycling

# 1. Introduction

The rising concerns about the energy crisis and environmental pollution have led to an urgent search for alternative green and renewable energy resources, including solar, wind, and tidal energy.[1, 2] Since renewable power sources are intrinsically intermittent, their integration into power systems inevitably generates some variability and uncertainty. Consequently, advanced electrochemical energy storage and conversion systems (e.g., supercapacitors, batteries, water splitting electrolyzers, and fuel cells) are highly desirable to achieve efficient utilization of green energy sources.[3, 4] Functional materials are the crucial components in the above systems.[5, 6] For instance, rechargeable batteries always require redox-active materials as solid electrodes as well as functional electrolytes to promote ion migration between the cathode and anode.[7] Energy conversion systems necessitate advanced electrode materials serving as both electron donor/acceptor and catalyst to accelerate the electrochemical reaction.[8] Therefore, the development of high-performance and low-cost electrode/electrolyte materials is a key prerequisite for the large-scale applications of electrochemical devices. And notably, increasing interests have been aroused to exploit battery materials and catalysts that can be produced with minimal environmental effect.[9, 10]

Deep eutectic solvents (DESs) are green liquid media obtained by mixing two or three components self-associated through hydrogen bond interactions.[11] As ionic liquid analogs, DESs share many characteristics, such as low vapor pressure, good thermal and chemical stability, non-flammability, and tunability.[11-13] Moreover, DESs possess additional merits comparing with ionic liquid, such as easy preparation, low expense, and nontoxicity.[11] DESs

have been the solvents of choice for the convenient synthesis of electroactive materials due to their chemical/thermal stability, and good solubility/dispersibility.[14] DESs can act as templates, carbon or metal sources, and as reactants or auxiliary agents in nanomaterial production. Owing to their non-flammability, large ionic conductivity, and wide electrochemical window, DESs have also be employed as reaction media for electrochemical deposition of nanomaterials [15] and electrolytes for electrochemical systems [16, 17]. All the above-mentioned advantages make DESs promising as functional electrolytes and precursors to advanced nanomaterials for green energy storage and conversion.

Up to date, there are a number of articles reviewing the potential applications of DESs in emerging fields including metal processing,[12] material chemistry,[13, 18, 19] electrochemistry,[20, 21] extraction/separation,[22, 23] and catalyst.[24] However, no report specifically summarizes the recent advances in DESs for energy storage and conversion. As shown in **Figure 1**a, we can see that this research field is booming in the past decade. We anticipate that a review article from the perspective of material science and engineering could open up a novel interdisciplinary field, which would push back the frontiers of knowledge for both DESs and green energy utilization. In this progress report, we first describe the fundamental physicochemical properties of DESs with those related to the green energy applications highlighted. Subsequently, the important roles that DESs play in various energy storage and conversion technologies are clarified, such as advanced electrolytes for batteries/supercapacitors, solvents for electrode material and catalyst synthesis, as well as extracting agent for battery recycling (Figure 1b). A special focus is paid on the fundamental understanding of their structure-composition-property-

performance relationships. Finally, the challenges, perspectives, and potential research directions are also discussed.

## 2. Properties of DESs

The increasing interest in DESs is attributed to their intriguing physicochemical properties, prospering many potential applications in different fields. DES is a mixture of at least two solid components, a hydrogen bond acceptor (HBA) and a hydrogen bond donor (HBD), having a lower melting point than each component. The difference between the freezing temperature at the eutectic composition of a binary mixture of A + B and that of a theoretical mixture, $\Delta T_f$, is illustrated in Figure 2a.[12] For instance, when ChCl and urea are mixed in a molar ratio of 1:2, the freezing point of the eutectic is 12 $^oC$, which is considerably lower than that of ChCl (303 $^oC$) and urea (134 $^oC$).[25]

As IL analogous, DESs share similar physical properties such as low vapor pressure, relatively wide liquid-range, good thermal stability, a wide electrochemical potential window, and nonflammability. So far, several reports have comprehensively reviewed the fundamental physicochemical properties of DESs. Herein we focus on the four most important parameters related to energy storage/conversion applications, including viscosity, ionic conductivity, electrochemical stability window, and solubility. Their potential impact on the electrochemical systems is highlighted.

## 2.1 Viscosity

The viscosity has a strong effect on the rate of mass transport within the solution; therefore, it is an important property determining the suitability of DESs for particular applications like electrochemical energy storage/conversion. The viscosity is closely related to intermolecular interactions in DES components. As a typical example, the LiTFSI/NMAc DES electrolyte has a lower viscosity compared to $LiPF_6$/NMAc and $LiNO_3$/NMAc since the $TFSI^-$ anion has a larger size and higher charge delocalization **(**Figure 2b).[26] It results in an accelerated lithium storage kinetics. Also, the HBD species play an important role in determining the viscosity. After replacing NMAc with Ace, the prepared LiTFSI/Ace eutectic had a higher viscosity close to 100 mPa·s (25 ºC) than 78.38 mPa·s of LiTFSI/NMAc.[26, 27] This is because the former has stronger hydrogen bonding than the latter. Except for the compositions of DESs, the temperature also significantly affects the viscosity properties. Generally, a negative correlation between two parameters is presented in DESs, which means a low viscosity can be acquired at a high temperature, and vice versa.[11]

When DESs are used as electrolytes for electrochemical systems, normally a high mass transfer rate is required, therefore a low viscosity is favorable. However, other safety-related parameters, like chemical/electrochemical/thermal stability, should also be seriously concerned for the DESs of choice.[28] A balance should be established among these parameters. As solvents for functional material synthesis, viscosity plays a significant role in tuning mass transport properties governing the genesis of nanostructures. Kumar-Krishnan reported that viscosity at different temperatures drives the growth of Au nanostructures into different shapes exhibiting high-index facets and stepped edges, thus affecting their catalytic performance to

$H_2O_2$ reduction.[29] For battery recycling, the viscosity of these DESs should be well controlled in order to improve the kinetics and efficiency.[30]

2.2 Ionic conductivity

Ionic conductivity is another crucial parameter that influences their applications in energy storage and conversion. As discussed above, the conductivity of DES generally increases as the temperature increases due to a decrease of DES' viscosity, and the relationship can be described using Vogel−Tamann−Fulher (VTF) equation. Taking the $Zn(TFSI)_2$/Ace system as an example, when the temperature increased from 25 to 80 $^oC$, the ionic conductivities of all DESs increased.[31] Therefore, when used DES as an electrolyte, the battery and supercapacitor generally have a higher capacity at a high temperature due to the improved ion transport kinetics. Additionally, changing the molar ratio of organic salt/HBDand tuning the species of salts or HBDs also significantly impact the conductivity of DES. As can be seen in Figure 2c, by increasing the HBD: Zn salt ratio from 4:1 to 9:1, the ionic conductivity of $Zn(TFSI)_2$/Ace DESs increased about 3 folds.[31] However, increasing the content of HBD may lead to side reactions in alkaline-metal batteries.

2.3 Electrochemical stability window (ESW)

Generally, the ESW is defined as the voltage difference between the cathodic and anodic limit, which is usually measured using cyclic voltammetry of linear scan voltammetry. Compared to the narrow ESW window of water (1.23 V), DESs are characterized by a much wider ESW, which allows them to be used as deposition media snd battery electrolytes. Many metal-based

electrocatalysts are prepared electrochemically using DESs because of the high ionic conductivity and high solubility of metal salts.

Owing to the wide ESW, DESs have been developed as new electrolytes high energy density devices. In general, the ESW of a DES has a close connection to the salt and water content. Cui et al. found that the $Zn(TFSI)_2$/Ace showed an expanded anodic stability limit of 2.4 V (vs. $Zn/Zn^{2+}$), outperforming those of DESs formed by other common Zn salts (*e.g.*, $Zn(ClO_4)_2$, $Zn(CH_3COO)_2$, and $Zn(BF_4)_2$) with different anions (Figure 2d).[31] Since DESs are water-miscible, the containing of water in DESs can significantly change many properties such as viscosity, ionic conductivity, and ESW. It was recently reported that the addition of a small amount of water almost didn't affect the ESW of DES because all water molecules were confined in the DES matrix via hydrogen-bonding.[32] Meanwhile, the conductivity of this "water-in-DES" electrolyte improved significantly, endowing Zn anode with unusual reversibility and durability. It should be noted that with excess water, such eutectic/$H_2O$ systems would change from a "water-in-eutectic" to an ordinary "aqueous solution" regime.

## 2.4 Solubility

Benefiting from the excellent solubility, DESs have been used to synthesize functional nanomaterials by electrochemical and chemical approaches for energy storage and conversion. Among different DESs, ChCl-based DESs are the most popular due to their excellent solubility of a large number of metal precursors, low cost, and negligible vapor pressures. Many metal precursors such as $NiCl_2{\cdot}6H_2O$, $FeCl_3{\cdot}6H_2O$, $CoCl_2{\cdot}6H_2O$, $H_2PtCl_6{\cdot}6H_2O$, and $La(NO_3)_3$ have shown high solubility in ChCl-based DESs for the synthesize of electrode materials and

electrocatalysts with special morphologies and properties.[33-36] Besides, DESs have much better dissolution power for organic compounds than water, which is very useful for the synthesis of carbonaceous materials. Very recently, multiple reports have demonstrated DESs' ability to dissolve common metal oxides, with certain compositions even rivaling the performance of acids. Therefore, DESs are recently attracted extensive attention for recycling valuable metals from spent batteries. Notably, increasing the temperature greatly enhanced the dissociation property of DESs, as verified by the increased metal ion concentration in the DESs.[37] Meanwhile, decreasing the molar ratio of salt:HBD is another feasible approach to increase solubility.[38]

## 3. DESs for energy storage applications

As discussed in the previous section, DESs have shown many attractive properties that are suitable for energy storage applications. For example, DESs prepared by mixing the Li salts with HBDs have been extensively studied as electrolytes for Li-ion and Li-metal batteries. Similar DES electrolytes were further extended to Zn and Al batteries in recent years. On the other hand, ChCl-based DESs have high ionic charge, high polarity, and low vapor pressure, they are feasible for the preparation of functional nanomaterials with special structures, resulting in the potential applications for electrode materials. Last but not least, thanks to the excellent solvation properties of DESs, they are applied for the leaching agents to recycle valuable metals such as cobalt in the spent Li-ion batteries (LIBs). In this section, the recent progress of DESs for energy storage applications will be discussed in detail.

## 3.1 DES-based electrolytes

Electrolyte plays a significant role in enabling the successful function of new electrode materials and chemistries. **Figure 3** compares various properties of the explored electrolytes, including DESs, organic liquids, ionic liquids, aqueous, polymers, and ceramic solids. Among them, organic liquid electrolytes are highly flammable and volatile, while the polymer and ceramic electrolytes suffer from poorer electrode/electrolyte interfacial contact than liquid-based ones. Based on the intrinsically high ionic conductivity, large metal-salt solubility, excellent electrochemical stability, and non-flammability, ILs fit well with most battery chemistries. Unfortunately, their practical applications are plagued by the high cost, difficulty in preparation, and toxicity. In contrast, DES-based electrolytes have gained increasing attention in various rechargeable batteries because they maintain the merits of ILs, and meanwhile, they are cheap, easy to prepare, and nontoxic. Yu et al. recently reviewed the use of eutectic electrolytes for energy storage devices with a special focus on redox flow batteries.[39] To avoid repeatability, here, we will only present the recent process of DESs as electrolytes for metal-based batteries and supercapacitors. The common physicochemical properties of various DES-based electrolytes, including freezing temperature, viscosity, and ionic conductivity, are summarized in **Table 1**.

### 3.1.1 Li-ion and Li-metal batteries

LIBs have been proven to be a transformative technology since their first commercial application in the 1990s.[40] They are characterized by a number of desired features for energy storage, including high energy density, low self-discharge, good rate capability, and long shelf-

life.[41-43] However, the use of highly flammable and volatile organic liquids as electrolytes causes severe safety concerns such as fire and explosion risks under abusive conditions (e.g., impact, overheating, and overcharging). Therefore, electrolytes characterized by low flammability, high ionic conductivity, good thermal stability, and low cost should be developed.[44] In this regard, versatile binary complex electrolytes based on the eutectic mixture of LiX salts (X = $TFSI^-$, $PF_6^-$, $ClO_4^-$, or different anions) and HBDs such as urea,[45] Ace,[27, 46] and NMAc [26, 47] are explored as electrolytes for non-aqueous lithium batteries. In 2013, Boisset et al. studied the physical/chemical properties of LiTFSI/NMAc DES electrolytes and evaluated their electrochemical performance for LIBs and supercapacitors.[47] The LiTFSI/NMAc electrolyte presented a room temperature conductivity close to 1.61 mS $cm^{-1}$ when the molar ratio of LiTFSI:NMAc is 1:4. At a high temperature of 150 $^oC$, the ionic conductivity increased to 28.4 mS $cm^{-1}$. More importantly, the DES maintains the liquid phase in a wide temperature range from –72 to 240 $^oC$, and thus it is promising for use at low temperatures. When it was used in $LiFePO_4$ (LFP)||Li battery, the cell delivered almost no capacity decay for 80 cycles at 80 $^oC$. These results confirmed that this DES has prominent advantages as an electrolyte due to its excellent thermal stability and safety with superionic character at elevated temperatures. Later on, the same group investigated three DES electrolytes containing different Li salts.[26] They found the $Li^+$ cations tend to coordinate with the C=O group of NMAc. The interaction between Li salts and NMAc weakens or even breaks the (N–H···O) hydrogen bond in NMAc, resulting in the formation of a eutectic mixture. Compared to $LiPF_6$ and $LiNO_3$, LiTFSI salt is easier to form a DES owing to the higher binding energy of $TFSI^-$ to metal ions. Besides, the

LiTFSI/NMAc system also had a lower viscosity than that of $LiPF_6$/NMAc and $LiNO_3$/NMAc, resulting in a higher ion transfer rate.

Despite liquid DESs being considered as “green” solvents in LIBs, confining DESs in the polymer matrix would be an attractive solution for leak-free, non-hazardous LIBs. Logan and co-workers reported a new class of safe, high-performance gel polymer electrolytes (GPEs) consisting of UV-cured acrylic polymers and a LiTFSI/NMAc DES (**Figure 4**a).[48] The eutectic GPEs exhibited improved electrochemical stability compared to the liquid DESs; however, their rate performance was still a bit poor. One should note that eutectic GPEs show significant non-flammability compared to liquid DESs attributed to the presence of polymer matrix. As shown in Figure 4b, when 1.5 wt% water is added in the eutectic GPE and pristine DES, the LMO||LTO full cell with eutectic GPE exhibits much better cyclic stability with 60% capacity retention after 200 cycles. Joos et al. came up with the design of eutectogels as a new class of solid composite electrolytes where the DES is confined within a silica matrix.[49] The transparent, homogeneous, glass-like eutectogel monoliths were fabricated by a nonaqueous sol-gel route. The optimized eutectogel electrolyte had an ionic conductivity of ∼1.5 mS $cm^{-1}$ at 25 °C, and the resulting LFP|| eutectogel electrolyte ||Li cell delivered a capacity of 105 mAh $g^{-1}$ at 0.1 C.

In addition, the DES electrolyte has also been used for high-energy-density aqueous LIBs. Jiang et al. fabricated a new DES consisting of methylsulfonylmethane (MSM), lithium perchlorate ($LiClO_4$), and water (Figure 4c).[50] The states of MSM/$LiClO_4$/$H_2O$ mixtures with different compositions are displayed in Figure 4d. When the molar ratios of MSM/$LiClO_4$ are maintained

between 2 and 3, the mixtures exhibit a stable liquid phase with an $H_2O$ amount between 0.3 and 1 in molar ratio. The obtained DES electrolyte is safe, environmentally friendly, low-cost, and it has a wide electrochemical stability window of ~3.5 V. The electrochemically stable DES (MSM:$LiClO_4$:$H_2O$ = 1.8:1:1) had a high ionic conductivity of 3.87 mS $cm^{-1}$ and was used as the electrolyte to construct a $LiMn_2O_4$ (LMO)||LTO aqueous LIB, which had a capacity retention of 72.2% after 1000 cycles at a high current of 4.5 C (Figure 4e).

Li metal offers a much higher specific capacity of 3860 mAh $g^{-1}$ and an extremely low electrode potential of −3.04 V vs. standard hydrogen electrode (SHE), making it an ideal anode for Li batteries.[51-53] However, the practical implementation of Li metal anode has been hampered by unstable solid electrolyte interphase (SEI) and uncontrollable dendritic growth, which lead to low Coulombic efficiency (CE), fast capacity fading, and even fatal safety concerns. Several eutectic electrolytes have been designed for Li metal anode to prevent Li dendrite growth [54, 55]. For example, Cui et al. reported succinonitrile (SN)-based dual-anion DES as a high-safety electrolyte for Li metal batteries.[55] The fabricated SN-based DES exhibited a high ionic conductivity of 2.86 mS $cm^{-1}$ with a large Li transfer number of 0.44 at 25 $^oC$, and good interfacial compatibility toward the Li metal. Moreover, the SN-based DES electrolyte showed negligible weight loss at 150 $^oC$ and non-flammability, in sharp contrast to the conventional carbonate electrolyte (**Figure 5**a,b). Finally, the as-prepared DES has been applied for high-voltage $LiCoO_2$||Li batteries, which exhibited impressive cycling stability and capacity retention of ~70% for 500 cycles with a cut-off voltage of 3.0−4.7 V. It is much superior to the cell using the commercial 1 M $LiPF_6$-EC/DMC electrolyte (negligible capacity after 150 cycles),

see Figure 5c. The reason can be attributed to the superior interfacial stability of SN-based dual-anion DES towards both lithium metal anode and high-voltage cathode, as confirmed by in-situ Fourier transform infrared spectroscopy (FTIR), X-ray photoelectron spectroscopy (XPS), and time-of-flight secondary ion mass spectrometry (TOF-SIMS). Therefore, optimization of the $Li^+$ solvation structure to reduce the free HBD molecules can alleviate the electrochemical performance of LMBs using DES electrolytes. The $LiCoO_2$||Li pouch cells could power an LED steadily even after the nail and corner-cut tests, implying the high safety of the SN-based DES electrolytes (Figure 5d).

The side reactions between Li and free HBD molecules may lead to large interfacial resistances. Therefore, the protection of Li metal via forming a stable SEI is a feasible approach. Recently, Zhou and co-workers developed a DES-based polymer (DSP) electrolyte which was synthesized in situ by thermally polymerizing 2-(3-(6-methyl-4-oxo-1,4-dihydropyrimidin-2-yl)ureido)ethyl methacrylate and pentaerythritol tetraacrylate monomers in the presence of a eutectic mixture of LiTFSI and NMAc with fluoroethylene carbonate (FEC) as an additive.[56] It is worth noting that the FEC additive not only improves the ionic conductivity and electrochemical stability of the polymer electrolyte but also promotes the formation of stable interfaces at both anode and cathode, preventing the Li dendrite growth on the anode side as well as the structural deterioration on the cathode side. In the meantime, the self-healing polymer matrix regulates the Li-ion flux and suppresses $Mn^{2+}$ dissolution from the Li transition metal oxide cathode (Figure 5e). Consequently, the DSP electrolyte enabled uniform Li deposition and high plating/stripping CEs, as confirmed by the Li||Li and Li||Cu testing results,

respectively. The electrochemical performance of LMO||Li full cells using the DSP and DES electrolytes are compared in Figure 5f. The one equipped with polymer electrolyte exhibited a reversible capacity of 99.5 mAh $g^{-1}$ after 200 cycles with a capacity retention of 86.1%, while the LMO||DES electrolyte||Li cell suffered from rapid capacity fading and failure after only 80 cycles.

3.1.2 Zn batteries

Zn batteries have been recently revisited and are highly desirable for large-scale energy-storage systems thanks to the large reserves of Zn, environmental friendliness, and intrinsic safety.[57-60]. Compared to alkali metals, Zn metal is insensitive to oxygen and humidity, which broadens the availability of electrolytes and lowers the processing costs.[61] Additionally, Zn metal exhibits a high volumetric capacity of 5855 Ah $L^{-1}$, superior to Li (2061 Ah $L^{-1}$), Ca (2072 Ah $L^{-1}$), and Mg (3833 Ah $L^{-1}$) counterparts.[57] However, the suboptimal cyclic efficiency resulting from uncontrolled dendrites and notorious side reactions occurring at the Zn-electrolyte interface (especially for aqueous electrolytes) restricts the development and application of rechargeable Zn batteries.[58, 59] There are some reports on polar-aprotic electrolytes (e.g., acetonitrile/Zn salt mixtures) for Zn batteries.[62, 63] Nevertheless, the acetonitrile is flammable, toxic, and volatile, reducing the overall stability of the battery. ILs seem to be a good choice, unfortunately, their high cost and sensitivity to moisture plague real-world applications.[64]

Recently, DESs were studied as electrolytes for Zn batteries because of their good stability in the air and moisture, low toxicity, low cost, and strong water-miscibility. For example,

Kheawhom et al. reported a biocompatible, stable, and low-cost ChCl/$ZnCl_2$/urea DES electrolyte.[65] No dendrites were found on the surface of Zn metal, suggesting the highly reversible plating/stripping behavior. With delta-type manganese oxide ($\delta$-$MnO_2$) as a cathode material, the Zn battery showed a fading rate of 0.7% per cycle. Although the CEs of ~90% at a current density of 100 mA $g^{-1}$ are not satisfactory, the above result indicates the great potential of the ChCl/$ZnCl_2$/urea electrolyte for Zn batteries. Currently, the application of $ZnCl_2$-based DES electrolytes is still hindered by their corrosivity toward common battery components, especially at high operating voltages. In another study, Cui et al. fabricated a stable and effective aqueous electrolyte by incorporating a small amount of water (~6 wt%) into a urea-based DES matrix.[32] As displayed in **Figure 6**a, the addition of water can lead to the formation of homogenous and clear solutions (described as LZ-DES/n$H_2O$; molar ratio: n = 0.5, 1, and 2). Among the LZ-DES/n$H_2O$ electrolytes, the LZ-DES/2$H_2O$ had a significantly reduced viscosity (139 mPa·s) and an enhanced conductivity (1.85 mS $cm^{-1}$) at 30 °C (Figure 6b). The in situ optical microscopy was used to compare the deposition of Zn in aqueous and DES electrolytes. As shown in Figure 6c, Zn deposition in 0.5 M LiTFSI + 0.5 M $Zn(TFSI)_2$ aqueous electrolyte shows serious gas bubbling, which significantly affects the uniform deposition. In contrast, the LZ-DES/n$H_2O$ is compatible with Zn metal, and no $H_2$ evolution was observed during the operando testing of Zn||Zn symmetric cells (Figure 6d). The plating/stripping curves in Figure 6e confirm the stability of Zn||Zn symmetric cells using the LZ-DES/2$H_2O$ electrolyte. And the Zn||$LiMnO_2$ battery showed excellent cyclic stability with capacity retention of 90.8% (after 300 cycles), 82.7% (after 600 cycles), and 86.6% (after 600 cycles) at 0.1 C, 0.5 C, and 2 C, respectively (Figure 6f). The ab initio molecular dynamics

(AIMD) calculations elucidated that no free water molecules were detected in both LZ-DES/1$H_2O$ and LZ-DES/2$H_2O$, suggesting that the LZ-DES/n$H_2O$ ($n \leq 2$) retains most of the eutectic essence.

As we mentioned before, water molecules can be incorporated to improve the conductivity and lower the viscosity of the DES electrolyte without destroying the DES nature in a controlled manner. However, when excess water is added, such eutectic/$H_2O$ systems would change from a "water-in-eutectic" to an ordinary "aqueous solution" regime.[66] Thus, precise control of the degree of hydration in DES via a cost-effective and facile approach is highly required. Very recently, a new class of hydrated eutectic Zn electrolytes (ZS) with a precise hydration level was prepared for Zn-organic battery through simply mixing a low-cost hydrated salt ($Zn(ClO_4)_2 \cdot 6H_2O$) with a neutral ligand of SN.[67] In such an electrolyte system, the Lewis basic SN essentially participates in the primary solvation shell of $Zn^{2+}$ ions with the formation of $[Zn(OH_2)_x(SN)_y]^{2+}$ cations, a hydration-deficient complex. The water molecules replaced by SN are bonded by SN in the outer solvation shell of $Zn^{2+}$ cations, contributing to the formation of the hydrated eutectic structure, as shown in Figure 6g. The SEM images shown in Figure 6h confirmed that the ZS electrolyte enabled a dendrite-free Zn plating/stripping, whereas the deposited Zn metal on the stainless-steel was uneven with many humps and holes when the $Zn(ClO_4)_2 \cdot 6H_2O/H_2O$ (ZW) electrolyte was employed (Figure 6i). The molecular dynamics simulations shown in Figure 6j revealed that the water molecules substituted by SN depart from the primary solvation shell of $Zn^{2+}$, which is also proved by the radial distribution function results. The sharp peak identified at 3.0 Å in the Zn-N pair suggests the containing of SN in the

primary solvation shell. Two peaks at 2.7 and 3.8 Å observed in the Zn-O imply the water molecules substituted by SN enter the second solvation shell (Figure 6k). The scarcity of free water in the ZS electrolyte restrains the dissolution of poly(2,3-dithiino-1,4-benzoquinone) (PDB); therefore, the PDB||ZS||Zn cell exhibits excellent charge-discharge cycling with a low degradation rate of 0.004% per cycle over 3500 cycles. More importantly, the eutectic nature of this aqueous electrolyte further guarantees stable low-temperature operation even at –20 °C (Figure 6l).

The stability of solid electrolyte interphase is one of the critical factors that affect the cycle life of rechargeable batteries. The Cui group presented the construction of zinc fluoride-rich organic/inorganic hybrid solid electrolyte interphase on zinc anode, based on a $Zn(TFSI)_2$/Ace eutectic electrolyte.[31] A large portion of $TFSI^-$ is found to coordinate to $Zn^{2+}$ directly in the form of anion-containing Zn complexes ($[ZnTFSI_m(Ace)_n]_{(2-m)}^+$, m = 1–2, n = 1–3), which induces the preferential reductive decomposition of $TFSI^-$ before Zn deposition. As a result, the in situ formed fluoride-rich SEI layer on the Zn surface enables high CE values (an average CE of 99.7% for 200 cycles) and uniform Zn plating/stripping at the areal capacity of > 2.5 mAh $cm^{-2}$, owing to the excellent Zn–electrolyte interfacial stability without the competing hydrogen evolution reaction (HER). Also, the fluoride-rich SEI remains stable when the battery is operated in a 1 M $Zn(TFSI)_2$ aqueous electrolyte, far superior to the pristine Zn without SEI protection. As expected, the cyclic stability of Zn||$V_2O_5$ cells using DES electrolyte ($Zn(TFSI)_2$:Ace = 1:7, molar ratio) outperforms their aqueous counterparts. Nevertheless, $Zn(TFSI)_2$-based DESs are expensive due to the high cost of $Zn(TFSI)_2$. Therefore, it is of great

interest to expand the types of salts and HBDs to further increase the overall properties of DES-based electrolytes.

### 3.1.3 Al batteries

Batteries based on Al offer a viable alternative to current LIBs because of Al's three-electron redox properties, low reduction potential (–2.3 V vs. SHE), stability in the metallic state, and very high natural abundance.[68] The development of these batteries based on non-flammable electrolytes with low toxicity is critical for minimizing the safety hazards and environmental impact. Based on the early work of Wilkes on chloroaluminate-based ILs such as $AlCl_3$/1-Ethyl-3-methylimidazolium chloride (EMIMCl),[69] Lin et al. recently developed an ultrafast rechargeable Al battery, which demonstrated a high energy density of 40 Wh $kg^{-1}$ at a high current density of 4 A $g^{-1}$ for more than 7500 cycles.[68] Unfortunately, these ILs are highly moisture sensitive and relatively expensive. Dai et al. pioneered the exploration of using a DES made from a mixture of $AlCl_3$ and urea in a 1.3:1 molar ratio for RT Al−graphite battery.[70] This battery displayed two discharge voltage plateaus around 1.9 and 1.5 V (average discharge = 1.73 V) and yielded a specific cathode capacity of ~73 mAh $g^{-1}$ at a current density of 100 mA $g^{-1}$ (~1.4 C). Besides, a high CE over a large range of charge-discharge rates and stability over ~150−200 cycles were also achieved. More importantly, they proposed that Al deposition proceeded through two possible pathways, one involving $Al_2Cl_7^-$ anions and the other involving $[AlCl_2 \cdot (urea)_n]^+$ cations. The intercalation of $AlCl_4^-$ into graphite was also confirmed, similar to that in the EMIMCl/$AlCl_3$ based Al battery. However, considering the high viscosity and low conductivity/ionicity, the DES electrolyte consisting of $AlCl_3$ and urea still needs

further improvement. In 2020, the same group investigated the conductivity and viscosity of $AlCl_3$/urea derivatives.[71] Significantly lower viscosity was realized, but the increase in conductivity was not as remarkable as expected. Therefore, highly conductive DESs for batteries need to be further explored.

Recent research on rechargeable Al–ion batteries has demonstrated stable and dendrite-free Al stripping and plating, and good cyclic stability property in chloroaluminate-based DESs. These DESs were then extended to rechargeable RT Al–S and Al–Se batteries.[72-74] Bian and co-workers developed an $AlCl_3$/urea DES electrolyte for RT Al–S batteries.[72] As sulfur is insoluble in the DES electrolyte, the charge/discharge cycle life of Al–S cells was improved. The Al–S cell delivered an initial capacity of 740 mAh $g^{-1}$ and had 85.3 % capacity retention (~520 mAh $g^{-1}$) after 100 charge-discharge cycles, which is superior to the results obtained using chloroaluminate-based ILs. Chu et al. also reported an $AlCl_3$/Ace electrolyte for RT Al–S batteries.[73] As shown in **Figure 7**a, the Al–S battery delivers an initial capacity of above 1500 mAh $g^{-1}$ and good rate performance (871 and 688 mAh $g^{-1}$ at 200 and 300 mA $g^{-1}$, respectively). The discharge capacity of Al–S batteries could maintain above 500 mAh $g^{-1}$ for 60 cycles at a current density of 100 mA $g^{-1}$ (Figure 7b). Besides, the reaction pathways proposed according to the XPS test and DFT calculations are illustrated in Figure 7c. Two possible pathways were proposed in Equations (1–4):

Pathway 1

Positive electrode: $8Al_2Cl_7^- + 3S + 6e^- \rightleftharpoons Al_2S_3 + 14AlCl_4^-$ (1)

Negative electrode: $2Al + 14AlCl_4^- - 6e^- \rightleftharpoons 8Al_2Cl_7^-$ (2)

Pathway 2

Positive electrode: $4[AlCl_2 \cdot (Ace)_2]^+ + 3S + 6e^- \rightleftharpoons Al_2S_3 + 2AlCl_4^-$ (3)

Negative electrode: $2Al + 2AlCl_4^- + 8\ Ace - 6e^- \rightleftharpoons 4[AlCl_2 \cdot (Ace)_2]^+$ (4)

Very similarly, an $AlCl_3$/thiourea DES was developed for rechargeable Al–Se batteries.[74] In such Al–Se batteries, Se nanowires grown directly on a flexible carbon cloth substrate (Se nanowires@CC) were used as the cathode material and Al foil was directly served as the anode. The Se nanowires@CC cathode delivered a high specific capacity of 260 mAh $g^{-1}$ at 50 mA $g^{-1}$ and maintained a long cycle life of 100 times with an average CE of nearly 93% at 100 mA $g^{-1}$. According to the Raman and XPS results, the reaction mechanisms of Al–Se in thiourea–$AlCl_3$ DES are analogous to those in Al–S batteries.

Al-air battery is another attractive device based on Al metal because of its high specific energy. Recently, Mori reported a DES-based solid electrolyte for rechargeable Al-air battery capable of removing the byproducts such as $Al_2O_3$ and $Al(OH)_3$ accumulates at both the anode and cathode.[75] The DES electrolyte was made by mixing $AlCl_3$, urea, carboxymethyl cellulose, and glycerin, while titanium nitride was used as the cathode. With this DES electrolyte, the Al-air battery delivered an initial capacity of 35.8 mAh $g^{-1}$ along with capacity retention of 97.8% for 50 cycles. In addition, other $AlCl_3$-based DESs were also developed for Al-air batteries. For example, the full-cell using $AlCl_3$/Ace (1:1.5) electrolyte displayed a current and energy efficiencies of 84% and 56% at 100 μA $cm^{-2}$ for 3 h, respectively.[76] Compared with the IL

electrolyte (i.e., EMIMCl), the Al-air battery equipped with the DES electrolyte showed better stability and higher voltage output. Although $AlCl_3$-based DESs have been widely used in Al batteries, new salts and new HBDs should be studied to further enhance the ionic conductivity and extend the electrochemical stability window.

### 3.1.4 Supercapacitors

The aqueous solution, organic solution, and ILs are the commonly used liquid electrolytes for supercapacitors. However, the aqueous electrolyte has a limited voltage window due to the decomposition of $H_2O$. Additionally, organic liquids are usually highly flammable and toxic, and ILs are expensive. As a consequence, green, safe, and low-cost DES electrolytes are being intensively investigated for safety- and energy-enhancing supercapacitors.[77-85] Besides, DES electrolytes can be operated at high temperatures, which is desired for some specific applications (e.g., military and aerospace). For example, Zaidi et al. proposed a new DES electrolyte based on sodium nitrate and NMAc for carbon-based supercapacitors at 80 °C.[86] The porous carbon-based supercapacitor delivered a high capacitance of ~100 F $g^{-1}$ at a current density of 200 mA $g^{-1}$, accompanying with a capacity retention of 80% for 1000 charge-discharge cycles. Further, Zhong et al. prepared a cheaper and safer DES consisting of ChCl and ethylene glycol (EG).[87] The stability of ChCl/EG DESs with different molar ratios (DES-1-1(ChCl: EF=1:1); DES-1-2 (1:2); DES-1-4 (1:4)) was first examined by comparing the binding energies. As shown in Figure 7d**,** the DES-1-2 showed the most negative value of –4.42 eV. The ionic conductivity increases with an increasing temperature ranging from RT to 115 °C, while the viscosity shows an opposite behavior (Figure 7e). The ChCl/EG DES can

operate normally over a wide temperature range from –40 to 115 °C, suggesting the good thermal stability of the DESs arising from the intramolecular hydrogen bonds (Figure 7f).

To enhance the ionic conductivity, Lien and co-workers introduced the co-solvents of water and acetonitrile into a typical DES electrolyte consisting of Ace and $LiClO_4$.[83] The addition of co-solvents not only resolves the limitations of high viscosity and low conductivity in DES but also improves the anti-freeze property and wettability. When the molar ratio of acetonitrile to water is 4.4:1, the hybrid DES shows the optimized physicochemical properties, including a wide ESW of 2.55 V, a superior conductivity of 15.6 mS $cm^{-1}$, and low viscosity of 5.82 mPa·s. Spectroscopic measurements confirmed that water molecules were strongly coordinated to $Li^+$ ions, thus resulting in a wide ESW. The symmetric supercapacitors with such hybrid DES electrolyte and $MoS_2$@reduced graphene oxide (SAED) hydrogel electrode delivered a maximum energy density of 31.2 Wh $kg^{-1}$ at a power density of 1164 W $kg^{-1}$ and exhibited ultralong cyclic stability of 20000 cycles.

Different gels composed of a DES and polymer matrix were also prepared as quasi-solid-state electrolytes for supercapacitors.[88, 89] An eco-friendly poly (vinyl alcohol)/Ace/$LiClO_4$ (PAL) DES-based gel electrolyte with a high ionic conductivity of ~12 mS $cm^{-1}$ was developed by adding PVA into the $LiClO_4$/Ace DES. It can be used for high-voltage wearable asymmetric supercapacitors (HVWASCs) with a large anodic voltage of 4.2 V,[88] and the HVWASCs exhibited outstanding energy density and power capability (245 Wh $kg^{-1}$ at 0.18 kW $kg^{-1}$ and 98 Wh $kg^{-1}$ at 95.3 kW $kg^{-1}$). Hong et al. locked the conductive DES in a double network ion gel for supercapacitor.[89] The ion gel was produced by the free radical polymerization of

acrylamide in a DES (composed of choline chloride, urea, and glycerol) and cellulose fiber mixture. Benefiting from the high ionic conductivity (0.58 mS $cm^{-1}$) and a wide operating voltage window (2 V) of DES-based ion gel, the fabricated supercapacitors exhibited a high specific capacitance of 76.6 F $g^{-1}$ at 1.0 A $g^{-1}$ and a high energy density of 10.64 Wh $kg^{-1}$ at a power density of 500 W $kg^{-1}$.

As mentioned above, DESs show intriguing properties, including high electrochemical stability, low toxicity, good thermal stability, low volatility, wider operating temperature range. Therefore, they are suitable as novel electrolytes for various batteries. However, the widespread use of DES electrolytes in conventional energy storage devices is currently limited because the ionic conductivity of DES electrolytes is about one order lower than the conventional liquid electrolytes, which greatly hinders the rate performance. Therefore, rational design of DES electrolytes with high ionic conductivity is needed. One common approach to improve ionic conductivity is to add a low-viscosity organic solvent. For example, the addition of FEC has been reported to improve the ionic conductivity and electrochemical stability of DESs against Li metal.[56] Besides, searching for new salts and new HBDs is crucial to enhance the ionic conductivity by lowering the viscosity. Another important aspect is that the side reactions between the alkali metal anodes and DES electrolyte still occur. Therefore, confining the DES liquid in the polymer matrix and reducing free HBD molecules can be attractive ways to minimize the incompatibility between DES electrolyte and highly reactive alkali metals.[55, 90]

## 3.2 Energy storage materials synthesized using DESs

Benefiting from the high ionic charge, high polarity, a supramolecular structure, and a high dielectric constant, DES is suitable for the synthesis of functional materials. DESs can be used as a green and safe solvent to electrodeposit metals on conductive substrates because of its excellent solubility to metal precursors. Besides, DESs can also function as reactants or precursors to prepare nanomaterials. For example, various carbon materials have been constructed using DESs as the precursor. Recently, DESs have also attracted interest in exfoliating layered nanomaterials. It should be noted that the research using DES to synthesize materials is still in its infancy, especially for materials related to energy storage applications. In this section, we focus on the DESs-based synthesis of functional materials for energy storage applications.

### 3.2.1 DESs as solvents for chemical and electrochemical synthesis of electrode materials

As mentioned in Section 2.2.4, DESs are a rising star as solvents to synthesize energy storage materials chemically and electrochemically because of their high ionic conductivity and low surface tension. Gu et al. reported the use of ethaline as a solvent to prepare core-shell nanoparticles comprising an amorphous Ni-P core and a crystalline $Ni_3P$ shell as prospective anode materials for LIBs.[91] In another study, nanostructured vanadium pentoxide ($V_2O_5$) with different morphologies were prepared by varying the water content in reline DES.[92] It was found that the alkyl amine based ionic species formed during the reline/water solvothermal treatment played a key role in the resulting material morphology. When pure water or pure reline was used as a solvent, similar random morphologies were obtained after solvothermal

synthesis, which was then converted into randomly arranged crystals (1D nanofleece) after calcination. Well-defined and uniform $V_2O_5$ hemihydrate ($V_2O_5 \cdot xH_2O$) microbeads were got in a 1:2 reline/water molar ratio mixture, and the $V_2O_5$ hemihydrate retained a similar shape after calcination.

Electrodeposition is another approach to synthesize nanomaterials from DESs for energy storage applications. With a setup of two or three electrodes, DESs have been successfully used as solvents (electrolytes) to prepare binder-free electrodes composed of electroactive metal films on conductive substrates. Except serving as the electrodeposition media, DESs are known to exhibit a stabilizing effect on the nanoparticles formed, and thus avoid the addition of any external stabilizer. Rao and co-workers demonstrated the electrodeposition of porous Sn-Ni-Cu alloy anode for LIBs in reline.[93] The deposition potential had a significant influence on the electrodeposition process and microstructure of the Sn-Ni-Cu alloy films. The Sn-Ni-Cu alloy film electrodeposited at −0.4 V in the Sn-Ni-Cu electrolyte shows a high reversible capacity of 533 mAh $g^{-1}$ after 50 cycles. Similarly, Co–Sn alloy film was also prepared and used as anodes for LIBs by pulse electrodeposition.[94] An obvious improvement in the cyclability appeared by adding Co as a matrix metal to the Sn film, although the surface morphology and the thickness of the deposit remain the same as those of the Sn film. Also, energy storage materials such as $LiMnPO_4$/C nanorods,[95] 3D hierarchical porous $NaTi_2(PO_4)_3$/C,[96] and Co-doped $Ni_3S_2$[97] have also been synthesized using DES as solvents.

3.2.2 DESs as reactants for chemical synthesis of electrode materials

Except as solvents, DESs commonly serve as a precursor for the fabrication of carbonaceous materials. Carbon-based materials synthesized using DES are advantageous: (1) DESs can direct the formation of pores during the synthesis procedure; (2) heteroatom doping can be easily obtained via the direct carbonization process. Francisco del Monte and co-workers pioneered the work in the synthesis of carbon materials from DESs. In 2010, they obtained monolithic carbon by carbonating the resorcinol–formaldehyde gel that was polymerized in ChCl:EG (1:2 in molar ratio)-type DESs.[98] The carbon derived from RF gel, synthesized in pure water, is dense with a surface area of 7 $m^2$ $g^{-1}$, a value much smaller than the one prepared from DES-type precursor (170 $m^2$ $g^{-1}$). Since resorcinol is an HBD, it can serve as a component to obtain DESs by mixing with ChCl.[99] This type of DES can act as both carbonaceous precursors and structure-directing agents that allow the preparation of hierarchically porous carbon monoliths via formaldehyde polycondensation and subsequent carbonization, with a carbon conversion of ~80%. Furthermore, they showed that hierarchical porous/CNT composites synthesized from DES have a high surface area and conductivity.[100] The porous/CNT composites retained 75% of the initial capacitance at a high current density of up to 765 mA $cm^{-2}$ (29 A $g^{-1}$).

Various intrinsic nitrogen (N)-doped carbons have been obtained by direct carbonization of DESs.[101-103] For example, N/O self-doped hollow carbon nanorods (HCNs) with micro/mesoporous walls are prepared using a new DES.[104] As shown in **Figure 8**a, the DES was obtained through the hydrogen-bond interactions among urea, 2,5-dihydroxy-1,4-

benzoquinone, and $ZnCl_2$. In such a DES, $ZnCl_2$ serves not only as a hydrogen-bond acceptor but also as a dehydration agent to promote the condensation process. During the carbonization process, $ZnCl_2$ also acts as a porogen by forming the ZnO template, and the evaporation of metallic Zn leads to the formation of porous HCNs. When assembling the HCN-based symmetric supercapacitor, the device exhibited a high energy density of 116.5 Wh $kg^{-1}$ at a power density of 472 W $kg^{-1}$.

Besides, ChCl/$Na_2S$ DES, together with graphene oxide (GO), has been used to prepare multi-functional S and N co-doped rGO.[105] Here, the DES was utilized as a solvent as well as a reducing agent and dopant. According to the elemental analysis, the S and N co-doped rGO composite had high S and N doping contents of 12.4 wt% and 4.9 wt%, respectively. When used as active materials in the supercapacitor, the S and N co-doped rGO electrode exhibited a high specific capacitance of 509 F $g^{-1}$ at 1 A $g^{-1}$, which corresponds to high energy and power densities of 57.3 Wh $kg^{-1}$ and 1804.7 W $kg^{-1}$, respectively.

DESs sometimes participate in chemical reactions for the synthesis of metal oxides and metal hydroxides.[106, 107] During the synthesis, the ammonia released from urea can react with the metal precursors and form a series of intermediates. After further treatment, different metal oxides and metal hydroxides can be obtained. Xiong et al. prepared $Fe_2O_3$ nanospindles composed of closely packed nanoparticles ionothermally in reline.[35] According to the scanning electron microscopy (SEM) and transmission electron microscopy (TEM) images, the uniform nanospindles have a size of ~ 180 nm, see Figure 8b,c. The selected area electron diffraction (SAED) pattern of a single nanospindle showed a single-crystalline nature (inset of Figure 8c).

When served as anode materials for LIBs, the as-prepared $Fe_2O_3$ nanospindles exhibited high capacity, good cycle stability (921.7 mAh $g^{-1}$ at 200 mA $g^{-1}$ for 50 cycles), and high rate capability (640.1 mAh $g^{-1}$ at 2000 mA $g^{-1}$).

Gu et al. reported the synthesis of nanoflower-like $\alpha$-$Ni(OH)_2$ in reline with a small amount of water.[108] As shown in Figure 8d, the TEM image confirmed the successful formation of nanoflower shape $\alpha$-$Ni(OH)_2$, which is composed of polycrystalline nanoflakes. The $Ni(OH)_2$ nanoflowers were further transformed to NiO by annealing and the obtained NiO had a large surface area of 72.9 $m^2$ $g^{-1}$. When used as an electrode for a supercapacitor, the NiO showed attractive specific capacitances of 555, 491, 422, and 311 F $g^{-1}$ at current densities of 2, 4, 8, and 20 A $g^{-1}$, respectively. Also, 2D $Co(OH)_2$ was prepared using a similar ionothermal strategy in a DES system.[109] A very large plane distance of about 11.2 Å was obtained in the $\alpha$-$Co(OH)_2$ sheets, leading to enhanced pseudocapacitive performance in alkaline aqueous media.

3.2.3 DESs as exfoliation agents for nanomaterials

Two-dimensional (2D) nanomaterials have shown great prospects in various research fields including energy storage, catalysis, sensing, electronics, etc.[110-112] DESs are known as green solvents having the advantages of nonflammability, high polarity, negligible vapor pressure, and easy recycling, and thus have been used as exfoliation agent to prepare single- or few-layer 2D materials. Abdelkader et al. reported the use of ChCl/urea system to exfoliate mechanochemically 2D crystals, including graphite, boron nitride, and transition metal dichalcogenides.[113] The exfoliation process was based on the co-intercalation of $Li^+$ and tetraethylammonium ions within the layered crystals using the shear forces in the milling

chamber. The produced materials are in majority of few-layer flakes with large lateral size. Besides, Mohammadpour et al. introduced sugar-based natural deep eutectic solvents as green intercalating solvents for the preparation of stable $MoS_2$ nanosheets.[114] Recently, they found that water can modulate the molecular arrangement of the DES and affect the synthesis efficiency of both $MoS_2$ and graphene nanosheets considerably.[115] It seems that the door of applying DESs to exfoliate 2D materials has just been opened. The green and low-cost DESs have great potential to replace the toxic organic solvents in preparing few-layer 2D materials.

In summary, DESs are advantageous in nanomaterial preparation for energy storage applications. Thanks to their high viscosity and high ionic strength, DESs can serve as a green solvent for the growth of functional nano-sized particles with special morphologies and structures. DESs can also participate in the chemical reactions and act as a reactant to obtain high-performance energy storage materials such as heteroatom doped carbon and transition metal compounds. The low vapor pressure allows the reaction to proceed at a high temperature and ambient pressure without the need for high-pressure reactors. Such a high temperature and ambient pressure protocol is safe and suitable for various chemical reactions. Besides, DESs are biodegradable, renewable, and non-toxic, making them environmentally friendly for large-scale applications.

## 3.3 Recycling of electrode materials using DESs

As another critical application, DESs have been regarded as effective leaching and reducing agents for extracting valuable elements from LIB waste. With the ever-increasing demand for

rechargeable LIBs, the accelerated production of these devices will soon translate into massive amounts of waste. Establishing effective LIB recycling strategies could balance the impact of end-of-life LIB waste and the demands on raw materials in the battery supply chain. For instance, the amount of Co and Li present in LIB cathodes could be as high as 15 and 7 wt%, respectively.[116, 117] The reuse of these metal elements from spent LIBs not only limits the risks of material shortages but also minimizes the impact of spent LIB waste on human health and the natural environment.

Common approaches to extracting the metal contained in the active lithium oxides are based on pyrometallurgy, hydrometallurgy, and a combination of the two.[118] Among them, pyrometallurgy is simple and feasible for large-scale applications. However, it is hampered by the high energetic cost from the extreme temperatures (1400 °C or higher) and the release of harmful gases. Hydrometallurgy is one of the most viable options, due to its high metal leaching rate and purity of the recovered product. Unfortunately, this technique usually involves caustic reagents such as hydrochloric, nitric, and sulfuric acids and requires a long processing time. DESs are a class of compounds that generally present an unusually high capability of dissolving metal oxides.[12] Therefore, it is intuitive to recover valuable elements from spent LIBs using DESs that provide suitable reducing and effective dissolving power for the desired elements.[119] Moreover, the low-cost and green nature of DESs are advantageous for real-world applications.

Ajayan et al. proposed a highly efficient method for Co extraction using a mixture of ChCl and EG.[120] The recycling process is schematically illustrated in **Figure 9**a. The battery was first dismantled, and the cathode waste was inserted into the DES. After heating and stirring, the

leachate can be filtered, and the other components (e.g., current collector, binder, and residual conductive carbon) can be recovered separately. Co compounds can then be recovered either through precipitation or electrodeposition, allowing the recovery of these valuable materials. The dissolution of Co was found to be highly dependent on the temperature in which the extraction occurred; the clear eutectic transformed into darker hues of blue at increased temperatures (Figure 9b) As shown in Figure 9c, Co leaching efficiencies were ~94.1% when the reaction temperature and time were 220 $^{o}$C and 24 h, respectively. The influence of reaction time was also examined (Figure 9d). It was found that at a temperature lower than 50 $^{o}$C, the improvement in leaching efficiency was relatively limited by extending the reaction time. Dissolved Co concentrations more than doubled from 24–48 h, and at a higher treatment temperature of 105 $^{o}$C. The extraction of Li and Co was also verified for the NMC cathode. Wang and co-workers used a reline mixture to extract Li and Co from spent LIBs (Figure 9e).[121] The strong reducibility of reline enabled the extraction at a mild condition (180 °C) with a short ethaline reaction time of 12 h. They also found Co can be recycled as $Co_3O_4$ using $H_2C_2O_4$ and NaOH precipitants using a dilution-precipitation-calcination process. Other DES systems such as ChCl/citric acid,[122] p-toluenesulfonic acid monohydrate/ChCl,[123] and polyethylene glycol/thiourea [124] were also studied for the recycling of $LiCoO_2$ in spent LIBs. In addition to the extraction of metal ions, Wang et al. reported a low-toxicity and low-cost DES for efficiently separating cathode materials from Al foil in spent LIBs.[125] The separation of the Al foil and cathode materials was achieved by the inactivation of the PVDF binder via a high-temperature alkali decomposition process in DES.

Using DESs to extract valuable metals from LIB waste is green and cheap.[118] DESs provide a green alternative to conventional methods of LIB recycling and reclaiming strategically important metals. However, to meet the requirements of large-scale applications, the processing time and capacity should be improved. To this end, rationally designed DESs are needed and the descriptors used to screen suitable DESs should be investigated. In addition, the affecting factor such as processing temperature, pH values, and reaction time need further optimization to maximize the economical benefits.

# 4. DESs for electrocatalytic applications

Electrolysis has experienced tremendous research interest over the past decade because of its important role in the production of renewable energies.[126] Various electrocatalytic reactions have been extensively investigated, including HER, oxygen evolution reaction (OER), methanol/ethanol oxidation reaction (MOR/EOR), oxygen reduction reaction (ORR), nitrogen reduction reaction (NRR), etc. In these electrochemical reactions, the conversion efficiency is critical to the performance of sustainable energy devices and is mainly determined by the electrocatalysts. Notably, the catalytic property relies heavily on the surface property of the materials; therefore, it is desirable to synthesize nanocatalysts with a high surface area and high-index facets, which could significantly enhance the catalytic activity. Benefiting from the multifunctional roles of DESs (solvents, soft template, structure-directing agents), they are becoming a versatile platform for the construction of high-performance electrocatalysts with specific structures and morphologies. In general, electrodeposition and wet-chemical reactions are the two most common approaches to synthesize electrocatalysts in DES systems. For

electrodeposition, the DESs serve as ionically conductive media that have high solubility of metal salts. In contrast, DESs function not only as a benign solvent but also as a reactant or precursor in the wet-chemical method. In the following section, we will present the recent development of high-performance electrocatalysts synthesized using DESs for various electrocatalytic reactions.

## 4.1 HER

For a catalytic reaction, the catalyst is a functional material used to reduce the overpotential and increase efficiency. HER is the reductive half-reaction of water electrolysis where protons obtain electrons to generate hydrogen gas in an aqueous media. Although Pt is regarded as the most efficient catalyst for HER, its high cost and low abundance hinder the wide application. Therefore, low-cost and high-performance alternatives should be explored.[127] Recently, electrodeposited nano-Ni films were prepared in the ChCl-based DES with $NiCl_2$ precursor for HER.[128] It has been observed that both the type of DES and the cathodic potential of electrodeposition affect the surface morphology of the deposited Ni films because the reduction of Ni(II) to Ni is a diffusion-controlled process. The Ni films with needle-like morphology (obtained in ChCl/EG system) showed improved HER durability and stability compared to the commercial Ni sheets. To increase the exposed surface area of catalysts, Yang et al. constructed Ni nanostructures on a nanoporous copper (NPC).[129] Owing to the abundant reaction sites, the 3D Ni architecture exhibited enhanced HER performance. Later on, they employed ethaline-based DESs to fabricate $Ni_3S_2$ on a nanoporous copper substrate because $Ni_3S_2$ is believed to show higher catalytic activity compared to Ni metal.[33] DESs here are

composed of $NiCl_2 \cdot 6H_2O$ and thiourea, which serve as nickel and sulfur sources, respectively. The fabrication process of nanoporous $Ni_3S_2$ films grown on the NPC template is shown in **Figure 10**a. Interestingly, the $O_2$ triggered the self-activation process of $Ni_3S_2$@NPC underwent in strongly acidic or basic media. Consequently, the activated $Ni_3S_2$@NPC showed excellent catalytic performance and stability over a wide range of pH, see Figure 10b-d. It also displayed high-performance HER catalytic activity in acidic media with robust durability over 111 h.

$MoS_2$ is another highly efficient HER catalyst. Mohammadpour et al. reported the preparation of stable $MoS_2$ nanosheets in a sugar-based natural DES.[114] It was found that the sugar-based DESs acted as intercalating solvents to assist the exfoliation of $MoS_2$. The as-prepared $MoS_2$ was in a mixed phase (2H−1T), as shown in the high-resolution TEM images (Figure 10e-g). The electrochemical results showed that the obtained 2H−1T $MoS_2$ nanosheets exhibited an overpotential of 0.339 V vs. reversible hydrogen electrode at the current density of 10 mA $cm^{-2}$ (Figures 10h) and long-term durability (2000 cycles) in acidic media (Figure 10i). However, it is worth mentioning that the yield is only about 44%, which is relatively low compared to other top-down exfoliation.

## 4.2 OER

OER is the oxidative half-reaction of water splitting, which usually shows sluggish kinetics due to the involvement of four-electron transfer process. Since the OER is the rate-limiting step, it is essential to develop cost-effective and high-performance OER catalysts or bifunctional catalysts to improve the overall efficiency of water splitting.[130-133] For example, DES (i.e.,

$CoCl_2 \cdot 6H_2O$ and urea) has been served simultaneously as a solvent, template, and reactant precursor to prepare two-dimensional (2D) $[Co(NH_3)_4CO_3]Cl$.[34] The obtained 2D $[Co(NH_3)_4CO_3]Cl$ nanosheets were then transformed into highly electroactive amorphous CoOOH through an activation process. The amorphous CoOOH catalyst displayed an excellent electrocatalytic activity with a low overpotential of 291 mV to reach a high current density of 10 mA $cm^{-2}$ and a low Tafel slope of 65 mV $dec^{-1}$. The authors claimed that the improved catalytic properties can be attributed to the 2D activated $[Co(NH_3)_4CO_3]Cl$, which increases the catalytic area and exposes more electrochemical active sites. Unfortunately, the formation mechanism of 2D architecture was not well revealed.

DESs have also been used to prepare advanced metal sulfide-based catalysts for OER. For instance, a multifunctional DES (as a solvent, shape-control agent, and sulfur source) composed of polyethylene glycol (PEG) 200 and thiourea was used for the solvothermal synthesis of nickel cobalt sulfide ($NiCo_2S_4$).[134] As shown in **Figure 11**a, the $NiCo_2S_4$ shows a spherical sea urchin-like micro-/nano-structure composed of uniformly interconnected nanorods. It also owns a high Brunauer–Emmett–Teller area, abundant active sites, easy diffusion of electrolytes and oxygen gas, and strong structural integrity. Consequently, the required overpotential was 337 mV to reach a current density of 10 mA $cm^{-2}$ (Figure 11b) and the Tafel slope was 64 mV $dec^{-1}$ (Figure 11c) in 1 M KOH. Moreover, $NiCo_2S_4$ demonstrated long-term stability with little deactivation after 2000 cycles. Thanks to the excellent solubility of various metal ions, Jiang et al. further fabricated a FeCoNi-based nitro-sulfide (FeCoNi-NS) hierarchical structure through the pyrolysis of multi-metal containing DES.[135] In specific, the DES composed of hydrated

metal salt ($FeCl_3 \cdot 6H_2O$, $CoCl_2 \cdot 6H_2O$, and $NiCl_2 \cdot 6H_2O$) and L-cysteine was prepared and then annealed at 350 °C for 12 h under $N_2$ atmosphere. The FeCoNi-NS displays much better OER performance (an overpotential of 251 mV at a current density of 10 mA $cm^{-2}$ and a low Tafel slope of 58 mV $dec^{-1}$ in 1 M KOH) than the single-metal counterparts (i.e., Fe-NS, Co-NS, and Ni-NS), which can be attributed to the synergy of the multi-metal sites.

The scalable water splitting requires high-performance and low-cost bifunctional catalysts (non-precious metal) for both HER and OER. As we mentioned before, nickel-based compounds are promising HER catalysts. Recently, an environment-friendly and one-step strategy was developed to fabricate 2D NiS/graphene heterostructure composites for water splitting. Novel DES composed of $NiCl_2$ and PEG200 was used as precursors for a pyrolysis accompanied sulfidation process.[136] Benefiting from the large specific surface area, the enhanced electrical conductivity, abundant surface-active sites, and long-term stability, the NiS/graphene shows excellent HER and OER performance (Figure 11d,e). A smaller cell voltage of 1.54 V was required to reach a current density of 10 mA $cm^{-2}$ with the NiS/graphene bifunctional catalysts compared to that use the $IrO_2$ (+)//Pt/C (−) counterpart (Figure 11f). Similarly, Mu et al. synthesized graphene encapsulated metal phosphides ($Ni_2P$@G) for electrocatalytic overall water splitting by annealing the designed DESs (consisting of $NiCl_2 \cdot 6H_2O$ and malonic acid) with $NiH_2PO_2 \cdot 2H_2O$.[137] DESs served as both a nickel source and carbon source for graphene formation. The geometrical limitation of metal nanoparticles within the graphene layer enhances their interfacial contact and inhibits dissolution and agglomeration of the nanoparticles, thus enhancing the hybrid's electrochemical activity and stability. The large exposed surface area of active

material along with the meso-/macro-porous feature promotes the easy utilization of the active catalytic sites. The Tafel slopes of $Ni_2P$@G for HER and OER are ~56.5 and 56.2 mV $dec^{-1}$, respectively. When used as a bifunctional catalyst in 1M KOH electrolyte, a bias voltage of 1.51 V is needed to achieve a water-splitting current density of 10 mA $cm^{-2}$. Recently, PCo nanoparticles[138] and Co-O@Co-Se films[139] were also constructed using designed DESs containing $Co^{2+}$ cations as the electrodeposition media. The electrodeposited Co-based catalysts showed good activity and durability for overall water splitting.

## 4.3 MOR/EOR

Direct alcohol fuel cells have been extensively studied for portable devices, owing to their high theoretical energy density (6.1 kWh $kg^{-1}$ for methanol and 8.6 kWh $kg^{-1}$ for ethanol), low toxicity, and capable of large-scale preparation of liquid fuels.[140] Nevertheless, serious problems prevent commercial adoption, including the sluggish electrode reaction kinetics, the poor long-term stability, and the high cost of noble metal electrocatalysts.[141] Typically, the rational design and elaborate synthesis of advanced electrocatalysts for the MOR and MER play a significant role in the development of commercially practical fuel cells. Regarding MOR, ethaline has been used as an electrolyte to electrodeposit Au@Pd nanoparticles.[142] The obtained Au@Pd nanoparticles displayed much higher activity than Au and Pd counterparts and demonstrated better tolerance to poisoning intermediates. Except for the electrodeposition method, a DES fabricated by dissolving $H_2PtCl_6$ and $CuSO_4$ in ChCl/EG was used to grow PtCu alloy nanoclusters on multi-walled carbon nanotubes (MWCNTs) via a solvent-thermal treatment (Figure 12f).[143] The incorporation of alloyed Cu atoms results in the formation of

cluster nanostructure with the coarse surface and it may also promote the electronic transfer interaction. As a result, $Pt_1Cu_{0.25}$/MWCNTs composite exhibited better MOR activity than Pt/MWCNTs catalysts (Figure 12g). The effect of Cu content on the electrochemical performance was evaluated and the results suggested that $Pt_1Cu_{0.25}$ showed the best MOR activity among different PtCu catalysts (PtCu mass ratios = 1:1, 1:0.67, 1:0.43, 1:0.25, and 1:0.11) that have been measured (Figure 12h). Other catalysts, such as Pt nanoparticles with a hollow-opened structure,[144] PtV alloys,[145] and carbon nanotube-supported PtCo catalysts,[146] were also prepared using DESs to promote the MOR activity.

Recently, a large spectrum of high-performance metal nanocrystal catalysts with high-index facets has been synthesized in DES media.[147-149] For example, Sun et al. synthesized concave tetrahexahedral Pt NCs with the {910} high-index through a simple electrodeposition method in chloroplatinic acid ($H_2PtCl_6$)-containing reline.[150] The Pt NC shape and atomic arrangement (surface structure) could be controlled simply by adjusting lower and upper potentials as illustrated by the cubic, truncated cubic, and concave cubic Pt NCs. The different shapes can be assigned to the selective and potential-dependent binding of urea to particular facets during growth. Owing to the high density of low-coordinated stepped atoms on their surfaces, tetrahexahedral Pt NCs exhibited enhanced catalytic activity for ethanol electro-oxidation. However, the size of as-prepared concave tetrahexahedral Pt NCs is at 100-nm scale, which may affect the utilization of expensive Pt catalysts. Furthermore, the same group reported concave cubic PtLa alloy NCs using ChCl/urea DESs for highly efficient ethanol electro-oxidation.[36] As shown in **Figure 12**a, the cubic PtLa alloy nanocrystals have a size of ~47.5 nm

with {410} high-index facets are successfully prepared. The scanning TEM (STEM) image and corresponding energy disperse X-ray (EDX) spectrometer elemental maps confirmed the uniform distribution of Pt and La elements in PtLa alloy NCs, see Figure 12b. The charge transfer interactions from La to Pt were probed by XPS spectra, in which a slightly positive shift (0.2 eV) for the Pt (0) state of the PtLa NCs was noticed, see Figure 12c. The synergetic effect of the high-index facets and the charge transfer interactions between Pt and La result in enhanced specific current activity and long-term durability for the EOR (Figure 12d,e). Au NCs with different morphologies (e.g., nanostars, nanodentists, and hierarchical nanoflowers) were also synthesized by changing the composition of DESs.[151] Notably, the water content in DESs has a significant impact on the final morphology. The resulting Au NCs exhibited high electrocatalytic activity and poisoning-resistance for ethanol electrooxidation in alkaline media.

## 4.4 ORR

ORR is a crucial process for fuel cells and commonly requires pt-based electrocatalysts.[152] So far, tremendous efforts have been paid to develop cost-efficient and outstanding electrocatalysts to replace the Pt-based electrocatalysts. Among various alternatives, pyridinic nitrogen (N) doped carbons attract significant attention because of their high stability and excellent activity.[126, 153] As mentioned in section 3.2, plenty of N-doped carbon materials can be prepared by using DESs as precursors. Therefore, it is intuitive to prepare ORR catalysts based on DESs because dopant and graphitization of carbon can be integrated tactfully. A DES containing tannic acid, urea, and zinc chloride was directly annealed at 700-1000 $^{o}$C to prepare N-doped graphitic carbon (**Figure 13**a,b).[154] In this DES, $ZnCl_2$ not only serves as the function

of a template but also promotes the precondensation process. The resulting NGCs possess large surface areas, rich N content, and high graphitization degree, resulting in excellent catalytic performance comparable to commercial Pt/C catalysts, as well as superior stability of 94.1% retention for 20000 s (Figure 13c). A scalable approach to produce $Fe_3O_4$/Fe doped graphene nanosheets ($Fe_3O_4$/Fe–GN) was also achieved by a DES generated by the complexation of ChCl and $FeCl_3$.[155] The $Fe_3O_4$/Fe–GN electrocatalyst demonstrated a positive onset potential, high cathodic current density, low hydrogen peroxide formation (<5%), and ideal 4-electron transfer for the whole potential range in alkaline media. Additionally, DESs can be also used as the reaction media for the synthesis of heteroatom doped carbon. By way of an example, N/P co-doped porous carbons were prepared by carbonation of free-standing polyaniline xerogels, which was prepared by DES-assisted oxidative polymerization.[156] During the preparation of polyaniline xerogels, DESs played an all-in-one role, being the solvent where the reaction was carried out and providing the monomer for polymerization in high concentration. The obtained polyaniline xerogels were then crosslinked by phytic acid and the N/P co-doped carbon monoliths were obtained by pyrolyzing the xerogels, which showed excellent ORR activity.

## 4.5 Other electrocatalytic reactions

Electrocatalytic NRR has been proposed as an alternative technology to generate $NH_3$ from $N_2$ and $H_2O$ under ambient conditions. Although the synthesis of $NH_3$ from $N_2$ and $H_2$ is exothermic under standard conditions, NRR is kinetically sluggish and contains complex multistep owing to difficult $N_2$ adsorption and N≡N cleavage.[157, 158] Designing novel electrocatalysts by lowering the $N_2$ reduction energy has been explored to surmount the barriers.

Recently, DES (PEG 200/thiourea)-derived $Fe_3S_4$ nanosheets were solvothermally fabricated to serve as a novel NRR electrocatalyst.[159] The DES not only serves as a shape controlling agents but also acts as a sulfur source, which is the key to the formation of $Fe_3S_4$ nanosheets (Figure 13d,e). The as-obtained $Fe_3S_4$ electrocatalyst was capable to reduce $N_2$ to $NH_3$ under ambient conditions and exhibited a high $NH_3$ yield (75.4 μg $h^{-1}$ $mg^{-1}_{cat.}$) and faradaic efficiency (6.45%) at −0.4 V vs. SHE (Figure 13f). Meanwhile, $Fe_3S_4$ nanosheets showed high selectivity without the detection of $N_2H_4$ by-product and good stability without an obvious decline in the current density at different potentials, see Figure 13g.

In addition to the above-mentioned electrocatalytic reactions, DESs have also been used to prepare catalysts for other reactions. Sun and co-workers synthesized high-index faceted Au NCs for glucose electro-oxidation.[160] Besides, various Au nanostructures were synthesized in reline and the effect of Au shape and surface area on their catalytic activity towards the reduction of $H_2O_2$ were examined.[29] Star-shaped Au nanoparticles with vicinal high-index facets were prepared by varying the water content in the DES (Figure 13h).[161] The star-shaped NPs showed excellent catalytic activity, with a 150 mV positive shift of the onset potential for $H_2O_2$reduction plus a 14-fold enhancement in reduction current density compared to that on a polycrystalline Au electrode, an outcome attributed to the presence of high-index facets (Figure 13i,j). Catalysts fabricated using DESs were applied for $CO_2$ reduction,[162] formic acid electrochemical oxidation,[130] urea electrolysis,[163] hydrazine oxidation[164].

DESs can be qualified as directing agents for controlling the synthesis of well-defined ordered nanocatalysts. Considering the high designability of DESs, various noble metals with unique

structures and high-index facets have been fabricated chemically or electrochemically. Besides, low-cost transition metal compounds and heteroatom-doped carbons were also prepared using DESs, which show good catalytic performance. However, the mechanistic understanding of the detailed chemistries during the synthesis is still lacking. Considering the demand for high-performance catalysts, DESs deserve further exploration and exploitation. New electrocatalysts are highly expected with the development of DESs.

## 5. Summary and Outlook

DESs have triggered a surge of interest and opened up appealing prospects in green energy applications since they share the remarkable qualities of both RTIL and green materials. In this review, recent important progress in this research field is systematically summarized, including DESs directly as advanced electrolytes for batteries/supercapacitors, as reaction media for synthesis of electrode materials/catalysts, and as extracting agents for battery recycling. A special focus is paid on the fundamental understanding of their structure-composition-property-performance relationships. Compared to other electrolyte systems, DESs have the advantages of high ionic conductivity, non-flammability as well as low cost and nontoxicity. The high concentration of DES electrolytes also enables the stabilization of electrolyte/electrode interfaces to broaden ESW and inhibits the dendrite formation in metal-based batteries. Therefore, DESs are promising electrolytes for fabricating cheap and safe energy storage devices. As reaction media for functional material synthesis, DESs can help produce morphology-controlled nanostructures, electrodeposited thin films, as well as hierarchically porous or heteroelement-doped carbon materials. They can serve multiple functions in the

nanosynthesis process such as supramolecular templates, carbon/metal sources, and oxidizing/reducing agents. DESs may also play an important role in regulating the nucleation/growth behaviors of nanocrystals. Through passivation of specific crystal planes, DESs can induce the preferred growth along particular crystallographic directions with high catalytic activities. Thus battery electrodes and catalysts with a variety of microstructures and electrochemical properties can be fabricated based on DESs. As recycling reagents, DESs can afford suitable reducing and effective dissolving capability for the desired elements. Moreover, the low-cost and green nature of DESs is a great merit for real-world applications.

In view of the current progress, the great potential of DESs for application in energy storage and conversion devices is apparent. However, substantial efforts are still required to overcome the remaining obstacles for the further development and practical application of DESs. The major challenges and future research directions are illustrated below.

DESs have been proposed as alternative electrolytes but they tend to exhibit inferior ionic conductivities due to their high viscosity in comparison to other liquid electrolytes. One promising approach is to introduce additives to enhance ion transportation while maintaining the eutectic essence. Some research results have emphasized that the addition of a small amount of water would have a significant improvement on the ionic conductivity of DESs, thus enabling fast reaction kinetics.[32] It should be noted that this approach is only feasible in aqueous batteries. In comparison, other additives need to be explored for alkali metal batteries. Besides, the ionic conductivity is also related to the components (i.e., HBAs and HBDs) and composition (i.e, the ratio of HBA to HBD). Therefore, new DES electrolytes need to be explored and

optimized as only a narrow range of DESs have been utilized as electrolytes. An additional challenge is the electrochemical stability of DESs against alkali metals is not satisfied yet. This may be resolved by developing functional additives and new HBDs. For example, Ogawa reported that it is preferable to design stable Li-salt/amide-based electrolytes using tetramethylurea without N–H bonds because the N–H bonds are unstable on the reduction side.[28] Besides, considering the complex structure of DESs, advanced ex-situ and in-situ characterizations along with modeling and simulations should be employed to better understand how the structure and dynamics of DES electrolytes affect the electrochemical and transport behavior. Without question, these results can provide new insights into the molecular features that lead to good (electro)chemical stability. Last but not least, the majority of literature is focused on Li batteries; it is interesting to replace the Li salts with other metal (e.g., sodium, calcium, and magnesium) salts, thus enabling the development of electrolytes for new chemistries beyond Li.

With regards to material fabrication, cheap and safe DESs have shown great potential in controlled nanoparticle synthesis, electrodeposition, and tailored porous carbons. DESs have been recognized to passivate particular crystal faces and dictate the preferred growth of nanocrystals along with specific crystallographic directions. However, the synthesis mainly depends on a trial-and-error process by tuning the variables (i.e., processing time, temperatures, water content, etc.). Substantial efforts should also be paid to elucidate the nucleation and growth mechanisms of nanocrystals using DESs. Additionally, ChCl/urea and ChCl/EG are the most commonly used DESs for material synthesis. In this regard, it is meaningful to explore

other DES systems, which will hasten progress in this area. Meanwhile, multiple essential parameters play significant roles in modulating species reactivity and mass transport properties governing the genesis of nanostructure, including viscosity, polarity, surface tension, hydrogen bonding, and coordination with solutes/surfaces. These parameters need sophisticated optimization to broaden the diversity of electrode materials and catalysts materials.

The high capability of dissolving metal oxides makes DES a good choice for recycling valuable metals from spent batteries. Lab-scale tests have demonstrated high purity and efficiency in metal recycling by using green and low-cost DESs. However, the processing time and capacity are not competitive in comparison to traditional methods. Considering the utilization of DESs for battery recycling is just springing up now, the following attempts may be considered to accelerate the real-world applications. Firstly, new DESs are needed and the descriptors used to screen suitable DESs for the effective recycling of spent LIBs should be investigated systematically. Artificial intelligence can contribute to screening different HBAs and HBDs, which can definitely promote the development of battery recycling. Secondly, the recycling process generally contains multiple steps, which evitably increase the cost. Therefore, the post-treatment to recovery and repurposing of the metal ions should be simplified. Thirdly, the environmental aspects of DESs after being employed were not assessed, and the recyclability of DESs is encouraged to be established.

In conclusion, DESs have shown great potential in resolving the challenges faced by electrochemical energy storage and conversion systems. Notably, the development of DESs is still in its infancy. The versatile types and functionalities of DESs will open new doors for

future development in the energy and environmental applications; therefore, more experimental and theoretical efforts are needed. Many more breakthroughs can be envisioned in this rapidly booming field.

# References


[1] J. M. Tour, C. Kittrell, V. L. Colvin, *Nat. Mater.,* **2010**, 9, 871-874.

[2] L. C. Stokes, C. Warshaw, *Nat. Energy,* **2017**, 2, 1-6.

[3] D. Larcher, J. M. Tarascon, *Nat. Chem.,* **2015**, 7, 19-29.

[4] M. A. Green, S. P. Bremner, *Nat. Mater.,* **2017**, 16, 23-34.

[5] W.-J. Liu, H. Jiang, H.-Q. Yu, *Energy Environ. Sci.,* **2019**, 12, 1751-1779.

[6] H. B. Wu, X. W. Lou, *Sci. Adv.,* **2017**, 3, eaap9252.

[7] J. B. Goodenough, K.-S. Park, *J. Am. Chem. Soc.,* **2013**, 135, 1167-1176.

[8] M. K. Debe, *Nature,* **2012**, 486, 43-51.

[9] T. Adschiri, Y.-W. Lee, M. Goto, S. Takami, *Green Chem.,* **2011**, 13, 1380-1390.

[10] M. Gao, C.-C. Shih, S.-Y. Pan, C.-C. Chueh, W.-C. Chen, *J. Mater. Chem. A,* **2018**, 6, 20546-20563.

[11] Q. Zhang, K. De Oliveira Vigier, S. Royer, F. Jérôme, *Chem. Soc. Rev.,* **2012**, 41, 7108-7146.

[12] E. L. Smith, A. P. Abbott, K. S. Ryder, *Chem. Rev.,* **2014**, 114, 11060-11082.

[13] D. V. Wagle, H. Zhao, G. A. Baker, *Acc. Chem. Res.,* **2014**, 47, 2299-2308.

[14] A. Abo-Hamad, M. Hayyan, M. A. AlSaadi, M. A. Hashim, *Chem. Eng. J.,* **2015**, 273, 551-567.

[15] A. P. Abbott, A. Ballantyne, R. C. Harris, J. A. Juma, K. S. Ryder, G. Forrest, *Electrochim. Acta,* **2015**, 176, 718-726.

[16] H. Cruz, N. Jordão, L. C. Branco, *Green Chem.,* **2017**, 19, 1653-1658.

[17] L. Bahadori, M. A. Hashim, N. S. A. Manan, F. S. Mjalli, I. M. AlNashef, N. P. Brandon, M. H. Chakrabarti, *J. Electrochem. Soc.,* **2016**, 163, A632-A638.

[18] L. I. N. Tomé, V. Baião, W. da Silva, C. M. A. Brett, *Appl. Mater. Today,* **2018**, 10, 30-50.

[19] X. Ge, C. Gu, X. Wang, J. Tu, *J. Mater. Chem. A,* **2017**, 5, 8209-8229.

[20] A. M. Navarro-Suárez, P. Johansson, *J. Electrochem. Soc.,* **2020**, 167, 070511.

[21] C. M. A. Brett, *Curr. Opin. Electrochem.,* **2018**, 10, 143-148.

[22] X. Li, K. H. Row, *J. Sep. Sci.,* **2016**, 39, 3505-3520.

[23] M. H. Zainal-Abidin, M. Hayyan, A. Hayyan, N. S. Jayakumar, *Anal. Chim. Acta,* **2017**, 979, 1-23.

[24] A. E. Ünlü, A. Arıkaya, S. Takaç, *Green Process. Synth.,* **2019**, 8, 355-372.

[25] A. P. Abbott, G. Capper, D. L. Davies, R. K. Rasheed, V. Tambyrajah, *Chem. Commun.,* **2003**, 70-71.

[26] A. Boisset, S. Menne, J. Jacquemin, A. Balducci, M. Anouti, *Phys. Chem. Chem. Phys.,* **2013**, 15, 20054-20063.

[27] Y. Hu, H. Li, X. Huang, L. Chen, *Electrochem. Commun.,* **2004**, 6, 28-32.

[28] H. Ogawa, H. Mori, *Phys. Chem. Chem. Phys.,* **2020**, 22, 8853-8863.

[29] S. Kumar-Krishnan, E. Prokhorov, O. Arias de Fuentes, M. Ramírez, N. Bogdanchikova, I. C. Sanchez, J. D. Mota-Morales, G. Luna-Bárcenas, *J. Mater. Chem. A,* **2015**, 3, 15869-15875.

[30] K. D. O. Vigier, G. Chatel, F. Jérôme, *ChemCatChem,* **2015**, 7, 1250-1260.

[31] H. Qiu, X. Du, J. Zhao, Y. Wang, J. Ju, Z. Chen, Z. Hu, D. Yan, X. Zhou, G. Cui, *Nat. Commun.,* **2019**, 10, 5374.

[32] J. Zhao, J. Zhang, W. Yang, B. Chen, Z. Zhao, H. Qiu, S. Dong, X. Zhou, G. Cui, L. Chen, *Nano Energy,* **2019**, 57, 625-634.

[33] C. Yang, M. Y. Gao, Q. B. Zhang, J. R. Zeng, X. T. Li, A. P. Abbott, *Nano Energy,* **2017**, 36, 85-94.

[34] S. Liu, C. Zhang, B. Zhang, Z. Li, J. Hao, *ACS Sustain. Chem. Eng.,* **2019**, 7, 8964-8971.

[35] Q. Q. Xiong, J. P. Tu, X. Ge, X. L. Wang, C. D. Gu, *J. Power Sources,* **2015**, 274, 1-7.

[36] S. Xiang, L. Wang, C.-C. Huang, Y.-J. Fan, H.-G. Tang, L. Wei, S.-G. Sun, *J. Power Sources,* **2018**, 399, 422-428.

[37] A. N. Dey, *Thin Solid Films,* **1977**, 43, 131-171.

[38] F. S. Ghareh Bagh, F. S. Mjalli, M. A. Hashim, M. K. O. Hadj-Kali, I. M. AlNashef, *J. Chem. Eng. Data,* **2013**, 58, 2154-2162.

[39] C. Zhang, L. Zhang, G. Yu, *Acc. Chem. Res.,* **2020**, 53, 1648-1659.

[40] A. Manthiram, *Nat. Commun.,* **2020**, 11, 1550.

[41] Z. Lu, F. Sui, Y.-E. Miao, G. Liu, C. Li, W. Dong, J. Cui, T. Liu, J. Wu, C. Yang, *J. Energy Chem.,* **2020**.

[42] J. Wu, X. Qin, H. Zhang, Y.-B. He, B. Li, L. Ke, W. Lv, H. Du, Q.-H. Yang, F. Kang, *Carbon,* **2015**, 84, 434-443.

[43] J. Wu, X. Qin, C. Miao, Y.-B. He, G. Liang, D. Zhou, M. Liu, C. Han, B. Li, F. Kang, *Carbon,* **2016**, 98, 582-591.

[44] J. Wu, J. Liu, Z. Lu, K. Lin, Y.-Q. Lyu, B. Li, F. Ciucci, J.-K. Kim, *Energy Storage Mater.,* **2019**, 23, 8-16.

[45] H. Liang, H. Li, Z. Wang, F. Wu, L. Chen, X. Huang, *J. Phys. Chem. B,* **2001**, 105, 9966-9969.

[46] R. Chen, F. Wu, B. Xu, L. Li, X. Qiu, S. Chen, *J. Electrochem. Soc.,* **2007**, 154, A703.

[47] A. Boisset, J. Jacquemin, M. Anouti, *Electrochim. Acta,* **2013**, 102, 120-126.

[48] M. W. Logan, S. Langevin, B. Tan, A. W. Freeman, C. Hoffman, D. B. Trigg, K. Gerasopoulos, *J. Mater. Chem. A,* **2020**, 8, 8485-8495.

[49] B. Joos, T. Vranken, W. Marchal, M. Safari, M. K. Van Bael, A. T. Hardy, *Chem. Mater.,* **2018**, 30, 655-662.

[50] P. Jiang, L. Chen, H. Shao, S. Huang, Q. Wang, Y. Su, X. Yan, X. Liang, J. Zhang, J. Feng, Z. Liu, *ACS Energy Lett.,* **2019**, 4, 1419-1426.

[51] K. Lin, X. Qin, M. Liu, X. Xu, G. Liang, J. Wu, F. Kang, G. Chen, B. Li, *Adv. Funct. Mater.,* **2019**, 29, 1903229.

[52] Y. Liu, X. Yin, X. Shen, P. Zou, X. Qin, C. Yang, Q. Zhang, F. Kang, G. Chen, B. Li, *Adv. Funct. Mater.,* **2020**, 30, 2002522.

[53] L. Zhang, X. Yin, S. Shen, Y. Liu, T. Li, H. Wang, X. Lv, X. Qin, S. W. Chiang, Y. Fu, F. Kang, B. Li, *Nano Lett.,* **2020**, 20, 5662-5669.

[54] H. Wu, B. Tang, X. Du, J. Zhang, X. Yu, Y. Wang, J. Ma, Q. Zhou, J. Zhao, S. Dong, G. Xu, J. Zhang, H. Xu, G. Cui, L. Chen, *Adv. Sci.,* **2020**, n/a, 2003370.

[55] Z. Hu, F. Xian, Z. Guo, C. Lu, X. Du, X. Cheng, S. Zhang, S. Dong, G. Cui, L. Chen, *Chem. Mater.,* **2020**, 32, 3405-3413.

[56] P. Jaumaux, Q. Liu, D. Zhou, X. Xu, T. Wang, Y. Wang, F. Kang, B. Li, G. Wang, *Angew. Chem. Int. Ed.,* **2020**, 59, 9134-9142.

[57] M. Song, H. Tan, D. Chao, H. J. Fan, *Adv. Funct. Mater.,* **2018**, 28, 1802564.

[58] D. Chao, W. Zhou, F. Xie, C. Ye, H. Li, M. Jaroniec, S.-Z. Qiao, *Sci. Adv.,* **2020**, 6, eaba4098.

[59] L. E. Blanc, D. Kundu, L. F. Nazar, *Joule,* **2020**, 4, 771-799.

[60] X. Jia, C. Liu, Z. G. Neale, J. Yang, G. Cao, *Chem. Rev.,* **2020**, 120, 7795-7866.

[61] F. Wang, W. Sun, Z. Shadike, E. Hu, X. Ji, T. Gao, X.-Q. Yang, K. Xu, C. Wang, *Angew. Chem. Int. Ed.,* **2018**, 57, 11978-11981.

[62] S.-D. Han, N. N. Rajput, X. Qu, B. Pan, M. He, M. S. Ferrandon, C. Liao, K. A. Persson, A. K. Burrell, *ACS Appl. Mater. Interfaces,* **2016**, 8, 3021-3031.

[63] N. Zhang, Y. Dong, Y. Wang, Y. Wang, J. Li, J. Xu, Y. Liu, L. Jiao, F. Cheng, *ACS Appl. Mater. Interfaces,* **2019**, 11, 32978-32986.

[64] T. J. Simons, D. R. MacFarlane, M. Forsyth, P. C. Howlett, *ChemElectroChem,* **2014**, 1, 1688-1697.

[65] W. Kao-ian, R. Pornprasertsuk, P. Thamyongkit, T. Maiyalagan, S. Kheawhom, *J. Electrochem. Soc.,* **2019**, 166, A1063-A1069.

[66] O. S. Hammond, D. T. Bowron, K. J. Edler, *Angew. Chem. Int. Ed.,* **2017**, 56, 9782-9785.

[67] W. Yang, X. Du, J. Zhao, Z. Chen, J. Li, J. Xie, Y. Zhang, Z. Cui, Q. Kong, Z. Zhao, C. Wang, Q. Zhang, G. Cui, *Joule,* **2020**, 4, 1557-1574.

[68] M.-C. Lin, M. Gong, B. Lu, Y. Wu, D.-Y. Wang, M. Guan, M. Angell, C. Chen, J. Yang, B.-J. Hwang, H. Dai, *Nature,* **2015**, 520, 324-328.

[69] J. S. Wilkes, J. A. Levisky, R. A. Wilson, C. L. Hussey, *Inorg. Chem.,* **1982**, 21, 1263-1264.

[70] M. Angell, C.-J. Pan, Y. Rong, C. Yuan, M.-C. Lin, B.-J. Hwang, H. Dai, *Proc. Natl. Acad. Sci.,* **2017**, 114, 834.

[71] M. Angell, G. Zhu, M.-C. Lin, Y. Rong, H. Dai, *Adv. Funct. Mater.,* **2020**, 30, 1901928.

[72] Y. Bian, Y. Li, Z. Yu, H. Chen, K. Du, C. Qiu, G. Zhang, Z. Lv, M.-C. Lin, *ChemElectroChem,* **2018**, 5, 3607-3611.

[73] W. Chu, X. Zhang, J. Wang, S. Zhao, S. Liu, H. Yu, *Energy Storage Mater.,* **2019**, 22, 418-423.

[74] S.-C. Wu, Y. Ai, Y.-Z. Chen, K. Wang, T.-Y. Yang, H.-J. Liao, T.-Y. Su, S.-Y. Tang, C.-W. Chen, D. C. Wu, Y.-C. Wang, A. Manikandan, Y.-C. Shih, L. Lee, Y.-L. Chueh, *ACS Appl. Mater. Interfaces,* **2020**, 12, 27064-27073.

[75] R. Mori, *RSC Adv.,* **2019**, 9, 22220-22226.

[76] N. Bogolowski, J.-F. Drillet, *Electrochim. Acta,* **2018**, 274, 353-358.

[77] S. Sathyamoorthi, N. Phattharasupakun, M. Sawangphruk, *Electrochim. Acta,* **2018**, 286, 148-157.

[78] W. Zaidi, A. Boisset, J. Jacquemin, L. Timperman, M. Anouti, *J. Phys. Chem. C,* **2014**, 118, 4033-4042.

[79] M. H. Mamme, S. L. C. Moors, H. Terryn, J. Deconinck, J. Ustarroz, F. De Proft, *J. Phys. Chem. Lett.,* **2018**, 9, 6296-6304.

[80] X. Bu, Y. Zhang, Y. Sun, L. Su, J. Meng, X. Lu, X. Yan, *J. Energy Chem.,* **2020**, 49, 198-204.

[81] V. K. Vorobiov, M. A. Smirnov, N. V. Bobrova, M. P. Sokolova, *Mater. Lett.,* **2021**, 283, 128889.

[82] M. Zhong, Q. F. Tang, Z. G. Qiu, W. P. Wang, X. Y. Chen, Z. J. Zhang, *J. Energy Storage,* **2020**, 32, 101904.

[83] C.-W. Lien, B. Vedhanarayanan, J.-H. Chen, J.-Y. Lin, H.-H. Tsai, L.-D. Shao, T.-W. Lin, *Chem. Eng. J.,* **2021**, 405, 126706.

[84] X. Bu, Y. Ge, L. Wang, L. Wu, X. Ma, D. Lu, *Polym. Eng. Sci.,* **2020**, n/a.

[85] K. T. T. Tran, L. T. M. Le, A. L. B. Phan, P. H. Tran, T. D. Vo, T. T. T. Truong, N. T. B. Nguyen, A. Garg, P. M. L. Le, M. V. Tran, *J. Mol. Liq.,* **2020**, 320, 114495.

[86] W. Zaidi, L. Timperman, M. Anouti, *RSC Adv.,* **2014**, 4, 45647-45652.

[87] M. Zhong, Q. F. Tang, Y. W. Zhu, X. Y. Chen, Z. J. Zhang, *J. Power Sources,* **2020**, 452, 227847.

[88] M.-J. Deng, T.-H. Chou, L.-H. Yeh, J.-M. Chen, K.-T. Lu, *J. Mater. Chem. A,* **2018**, 6, 20686-20694.

[89] S. Hong, Y. Yuan, C. Liu, W. Chen, L. Chen, H. Lian, H. Liimatainen, *J. Mater. Chem. C,* **2020**, 8, 550-560.

[90] C. Wang, H. Zhang, S. Dong, Z. Hu, R. Hu, Z. Guo, T. Wang, G. Cui, L. Chen, *Chem. Mater.,* **2020**.

[91] H. Zhang, Y. Lu, C.-D. Gu, X.-L. Wang, J.-P. Tu, *CrystEngComm,* **2012**, 14, 7942-7950.

[92] S. Datta, C. Jo, M. De Volder, L. Torrente-Murciano, *ACS Appl. Mater. Interfaces,* **2020**, 12, 18803-18812.

[93] S. Rao, X. Zou, S. Wang, T. Shi, Y. Lu, L. Ji, H.-Y. Hsu, Q. Xu, X. Lu, *J. Electrochem. Soc.,* **2019**, 166, D427-D434.

[94] K. Ui, S. Kikuchi, Y. Jimba, N. Kumagai, *J. Power Sources,* **2011**, 196, 3916-3920.

[95] Z. Wu, R.-R. Huang, H. Yu, Y.-C. Xie, X.-Y. Lv, J. Su, Y.-F. Long, Y.-X. Wen, *Materials,* **2017**, 10.

[96] F. Jiang, Y. Zhou, J. Su, Y.-F. Long, X.-Y. Lv, Y.-X. Wen, *Ionics,* **2020**.

[97] J. R. Zeng, L. Chen, S. S. Siwal, Q. B. Zhang, *Sustain. Energy Fuels,* **2019**, 3, 1957-1965.

[98] M. C. Gutiérrez, F. Rubio, F. del Monte, *Chem. Mater.,* **2010**, 22, 2711-2719.

[99] D. Carriazo, M. C. Gutiérrez, M. L. Ferrer, F. del Monte, *Chem. Mater.,* **2010**, 22, 6146-6152.

[100] M. C. Gutiérrez, D. Carriazo, A. Tamayo, R. Jiménez, F. Picó, J. M. Rojo, M. L. Ferrer, F. del Monte, *Chem. Eur. J.,* **2011**, 17, 10533-10537.

[101] L. Chen, J. Deng, Y. Song, S. Hong, H. Lian, *Mater. Res. Bull.,* **2020**, 123, 110708.

[102] R. Zhou, C. Xu, J. Yang, D. Guan, J. Cai, *Chem. Lett.,* **2020**, 49, 585-588.

[103] M. C. Gutiérrez, D. Carriazo, C. O. Ania, J. B. Parra, M. L. Ferrer, F. del Monte, *Energy Environ. Sci.,* **2011**, 4, 3535-3544.

[104] D. Xue, D. Zhu, H. Duan, Z. Wang, Y. Lv, W. Xiong, L. Li, M. Liu, L. Gan, *Chem. Commun.,* **2019**, 55, 11219-11222.

[105] P. H. Wadekar, R. V. Khose, D. A. Pethsangave, S. Some, *ChemSusChem,* **2019**, 12, 3326-3335.

[106] K. Aruchamy, N. Maalige R, M. Halanur M, A. Mahto, R. Nagaraj, D. Kalpana, D. Ghosh, D. Mondal, S. K. Nataraj, *Chem. Eng. J.,* **2020**, 379, 122327.

[107] G. M. Thorat, H. S. Jadhav, W.-J. Chung, J. G. Seo, *J. Alloys Compd.,* **2018**, 732, 694-704.

[108] X. Ge, C. D. Gu, Y. Lu, X. L. Wang, J. P. Tu, *J. Mater. Chem. A,* **2013**, 1, 13454-13461.

[109] X. Ge, C. D. Gu, X. L. Wang, J. P. Tu, *J. Phys. Chem. C,* **2014**, 118, 911-923.

[110] J. Wu, Z. Lu, K. Li, J. Cui, S. Yao, M. Ihsan-ul Haq, B. Li, Q.-H. Yang, F. Kang, F. Ciucci, J.-K. Kim, *J. Mater. Chem. A,* **2018**, 6, 5668-5677.

[111] J. Wu, M. Ihsan-Ul-Haq, F. Ciucci, B. Huang, J.-K. Kim, *Energy Storage Mater.,* **2021**, 34.

[112] J. Wu, F. Ciucci, J.-K. Kim, *Chem. Eur. J.,* **2020**, 26, 6296-6319.

[113] A. M. Abdelkader, I. A. Kinloch, *ACS Sustain. Chem. Eng.,* **2016**, 4, 4465-4472.

[114] Z. Mohammadpour, S. H. Abdollahi, A. Safavi, *ACS Appl. Energy Mater.,* **2018**, 1, 5896-5906.

[115] Z. Mohammadpour, S. H. Abdollahi, A. Omidvar, A. Mohajeri, A. Safavi, *J. Mol. Liq.,* **2020**, 309, 113087.

[116] X. Chen, J. Li, D. Kang, T. Zhou, H. Ma, *Green Chem.,* **2019**, 21, 6342-6352.

[117] X. Chen, D. Kang, J. Li, T. Zhou, H. Ma, *J. Hazard. Mater.,* **2020**, 389, 121887.

[118] X. Zheng, Z. Zhu, X. Lin, Y. Zhang, Y. He, H. Cao, Z. Sun, *Engineering,* **2018**, 4, 361-370.

[119] I. M. Pateli, A. P. Abbott, G. R. T. Jenkin, J. M. Hartley, *Green Chem.,* **2020**.

[120] M. K. Tran, M.-T. F. Rodrigues, K. Kato, G. Babu, P. M. Ajayan, *Nat. Energy,* **2019**, 4, 339-345.

[121] S. Wang, Z. Zhang, Z. Lu, Z. Xu, *Green Chem.,* **2020**, 22, 4473-4482.

[122] N. Peeters, K. Binnemans, S. Riaño, *Green Chem.,* **2020**, 22, 4210-4221.

[123] M. J. Roldán-Ruiz, M. L. Ferrer, M. C. Gutiérrez, F. d. Monte, *ACS Sustain. Chem. Eng.,* **2020**, 8, 5437-5445.

[124] Y. Chen, Y. Lu, Z. Liu, L. Zhou, Z. Li, J. Jiang, L. Wei, P. Ren, T. Mu, *ACS Sustain. Chem. Eng.,* **2020**, 8, 11713-11720.

[125] M. Wang, Q. Tan, L. Liu, J. Li, *J. Hazard. Mater.,* **2019**, 380, 120846.

[126] J. Wang, H. Kong, J. Zhang, Y. Hao, Z. Shao, F. Ciucci, *Prog. Mater. Sci.,* **2020**, 100717.

[127] K. Kopczyński, G. Lota, *Electrochem. Commun.,* **2019**, 107, 106538.

[128] S. Wang, X. Zou, Y. Lu, S. Rao, X. Xie, Z. Pang, X. Lu, Q. Xu, Z. Zhou, *Int. J. Hydrog. Energy,* **2018**, 43, 15673-15686.

[129] C. Yang, Q. B. Zhang, A. P. Abbott, *Electrochem. Commun.,* **2016**, 70, 60-64.

[130] C. Zhang, T. Chen, H. Zhang, Z. Li, J. Hao, *Chem. Asian. J.,* **2019**, 14, 2995-3002.

[131] A. Verma, D. P. Jaihindh, Y.-P. Fu, *Dalton Trans.,* **2019**, 48, 8594-8610.

[132] G. M. Thorat, H. S. Jadhav, A. Roy, W.-J. Chung, J. G. Seo, *ACS Sustain. Chem. Eng.,* **2018**, 6, 16255-16266.

[133] X. Zhao, J. Jiang, Z. Xue, C. Yan, T. Mu, *Chem. Commun.,* **2017**, 53, 9418-9421.

[134] J. Jiang, C. Yan, X. Zhao, H. Luo, Z. Xue, T. Mu, *Green Chem.,* **2017**, 19, 3023-3031.

[135] J. Jiang, L. Chang, W. Zhao, Q. Tian, Q. Xu, *Chem. Commun.,* **2019**, 55, 10174-10177.

[136] D. Zhang, H. Mou, F. Lu, C. Song, D. Wang, *Appl. Catal. B Environ.,* **2019**, 254, 471-478.

[137] H. Mou, J. Wang, D. Yu, D. Zhang, F. Lu, L. Chen, D. Wang, T. Mu, *J. Mater. Chem. A,* **2019**, 7, 13455-13459.

[138] K. Li, T.-z. Ren, Z.-Y. Yuan, T. J. Bandosz, *Int. J. Hydrog. Energy,* **2018**, 43, 10448-10457.

[139] W. Q. Yang, Y. X. Hua, Q. B. Zhang, H. Lei, C. Y. Xu, *Electrochim. Acta,* **2018**, 273, 71-79.

[140] C. Lamy, A. Lima, V. LeRhun, F. Delime, C. Coutanceau, J.-M. Léger, *J. Power Sources,* **2002**, 105, 283-296.

[141] C. Bianchini, P. K. Shen, *Chem. Rev.,* **2009**, 109, 4183-4206.

[142] A. Renjith, V. Lakshminarayanan, *J. Mater. Chem. A,* **2015**, 3, 3019-3028.

[143] J. Zhong, L. Li, M. Waqas, X. Wang, Y. Fan, J. Qi, B. Yang, C. Rong, W. Chen, S. Sun, *Electrochim. Acta,* **2019**, 322, 134677.

[144] X. Wang, M. Sun, S. Xiang, M. Waqas, Y. Fan, J. Zhong, K. Huang, W. Chen, L. Liu, J. Yang, *Electrochim. Acta,* **2020**, 337, 135742.

[145] J.-M. Zhang, J.-J. He, X.-Q. Wang, Y.-J. Fan, X.-J. Zhang, J.-P. Zhong, W. Chen, S.-G. Sun, *Int. J. Hydrog. Energy,* **2019**, 44, 28709-28719.

[146] J.-M. Zhang, S.-N. Sun, Y. Li, X.-J. Zhang, P.-Y. Zhang, Y.-J. Fan, *Int. J. Hydrog. Energy,* **2017**, 42, 26744-26751.

[147] L. Wei, Y.-J. Fan, H.-H. Wang, N. Tian, Z.-Y. Zhou, S.-G. Sun, *Electrochim. Acta,* **2012**, 76, 468-474.

[148] L. Wei, Z.-Y. Zhou, S.-P. Chen, C.-D. Xu, D. Su, M. E. Schuster, S.-G. Sun, *Chem. Commun.,* **2013**, 49, 11152-11154.

[149] L. Wei, K. Liu, Y.-J. Mao, T. Sheng, Y.-S. Wei, J.-W. Li, X.-S. Zhao, F.-C. Zhu, B.-B. Xu, S.-G. Sun, *Phys. Chem. Chem. Phys.,* **2017**, 19, 31553-31559.

[150] L. Wei, Y.-J. Fan, N. Tian, Z.-Y. Zhou, X.-Q. Zhao, B.-W. Mao, S.-G. Sun, *J. Phys. Chem. C,* **2012**, 116, 2040-2044.

[151] A. Li, Y. Chen, K. Zhuo, C. Wang, C. Wang, J. Wang, *RSC Adv.,* **2016**, 6, 8786-8790.

[152] J. Wang, Y. Gao, H. Kong, J. Kim, S. Choi, F. Ciucci, Y. Hao, S. Yang, Z. Shao, J. Lim, *Chem. Soc. Rev.,* **2020**.

[153] J. Wang, J. Kim, S. Choi, H. Wang, J. Lim, *Small Methods,* **2020**, 4, 2000621.

[154] R. Luo, C. Liu, J. Li, C. Wang, X. Sun, J. Shen, W. Han, L. Wang, *ACS Appl. Mater. Interfaces,* **2017**, 9, 32737-32744.

[155] D. Mondal, M. Sharma, C.-H. Wang, Y.-C. Lin, H.-C. Huang, A. Saha, S. K. Nataraj, K. Prasad, *Green Chem.,* **2016**, 18, 2819-2826.

[156] R. J. Sánchez-Leija, N. López-Salas, J. L. G. Fierro, M. C. Gutiérrez, M. L. Ferrer, J. D. Mota-Morales, G. Luna-Bárcenas, F. d. Monte, *Carbon,* **2019**, 146, 813-826.

[157] W. Xu, G. Fan, J. Chen, J. Li, L. Zhang, S. Zhu, X. Su, F. Cheng, J. Chen, *Angew. Chem. Int. Ed.,* **2020**, 132, 3539-3544.

[158] F. Lai, W. Zong, G. He, Y. Xu, H. Huang, B. Weng, D. Rao, J. A. Martens, J. Hofkens, I. P. Parkin, *Angew. Chem. Int. Ed.,* **2020**, 132, 13422-13429.

[159] X. Zhao, X. Lan, D. Yu, H. Fu, Z. Liu, T. Mu, *Chem. Commun.,* **2018**, 54, 13010-13013.

[160] L. Wei, T. Sheng, J.-Y. Ye, B.-A. Lu, N. Tian, Z.-Y. Zhou, X.-S. Zhao, S.-G. Sun, *Langmuir,* **2017**, 33, 6991-6998.

[161] H.-G. Liao, Y.-X. Jiang, Z.-Y. Zhou, S.-P. Chen, S.-G. Sun, *Angew. Chem. Int. Ed.,* **2008**, 47, 9100-9103.

[162] B. Bohlen, D. Wastl, J. Radomski, V. Sieber, L. Vieira, *Electrochem. Commun.,* **2020**, 110, 106597.

[163] H. Zhang, K. Lu, B. Li, Y. Liu, Y. Su, R. Wang, Y. Cheng, *ACS Appl. Mater. Interfaces,* **2020**, 12, 42704-42710.

[164] M. Tohidi, F. A. Mahyari, A. Safavi, *RSC Adv.,* **2015**, 5, 32744-32754.

[165] A. P. Abbott, R. C. Harris, K. S. Ryder, *J. Phys. Chem. B,* **2007**, 111, 4910-4913.

[166] A. P. Abbott, J. C. Barron, K. S. Ryder, D. Wilson, *Chem. Eur. J.,* **2007**, 13, 6495-6501.

[167] Y. Hu, Z. Wang, X. Huang, L. Chen, *Solid State Ion.,* **2004**, 175, 277-280.

# Acknowledgments

# Figures and tables

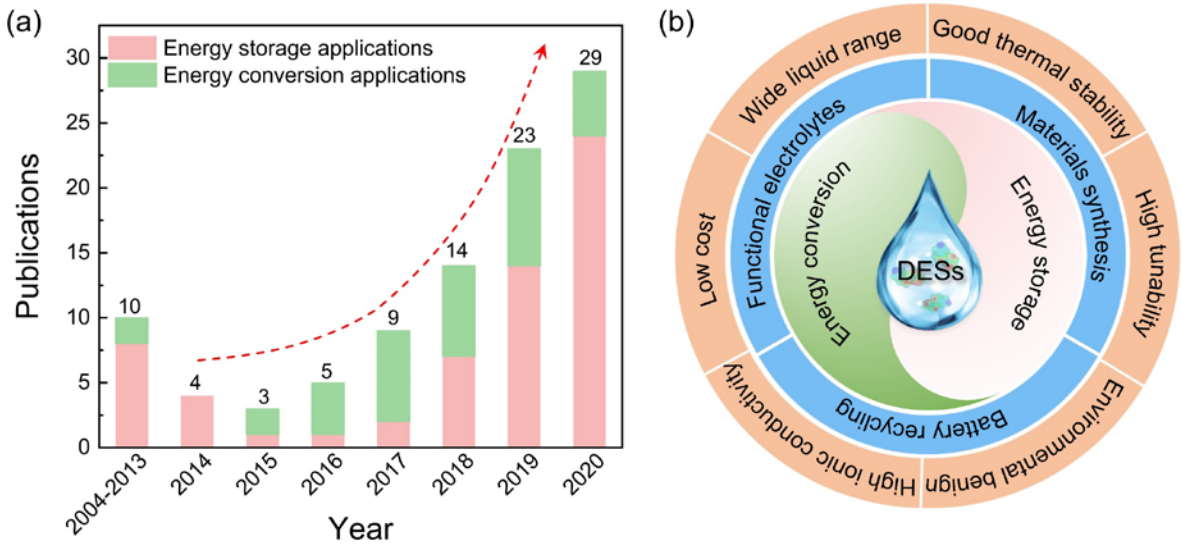


**Figure 1.** a) Research papers of DESs for energy storage and conversion applications from 2004 to November 2020. b) Overview of the properties of DESs and their applications in energy storage and conversion fields.

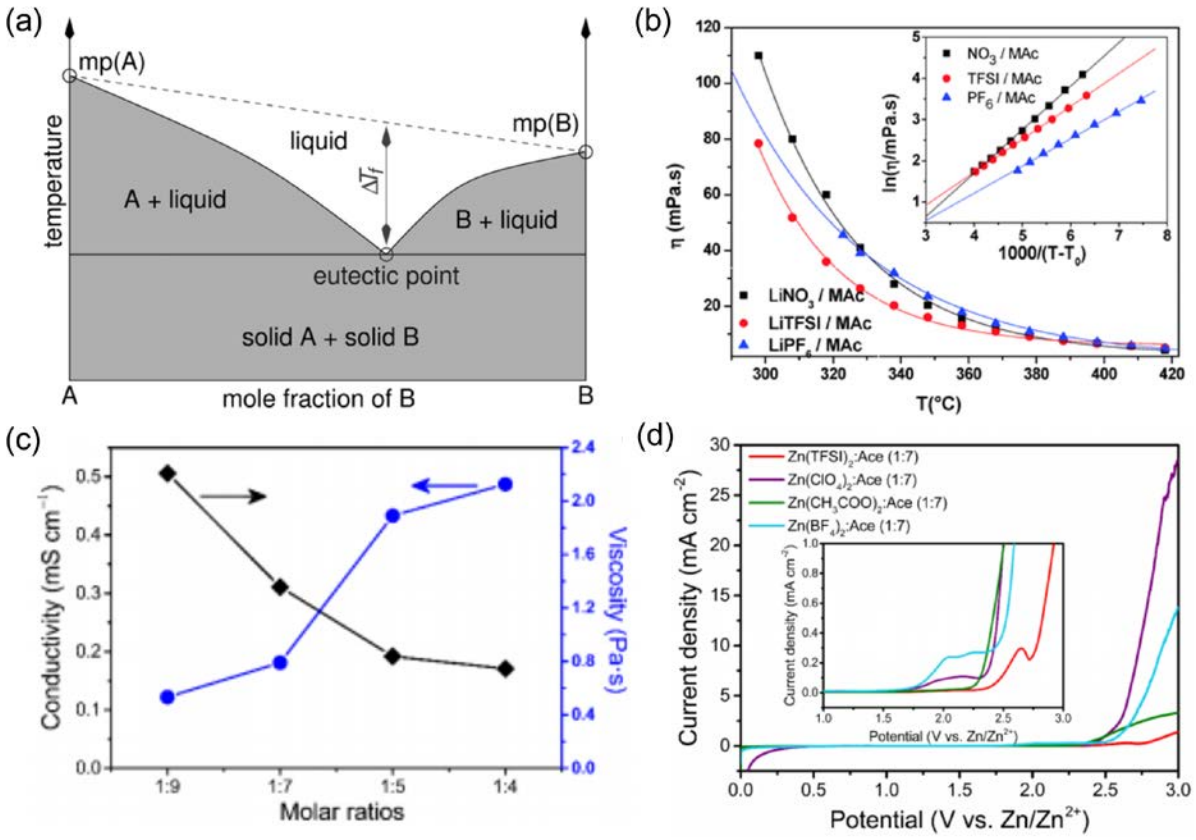


**Figure 2.** a) Schematic illustration of a eutectic point on a two-component phase diagram. Reproduced with permission. [12] Copyright 2014, American Chemical Society. b) the viscosity versus temperature curves for $LiNO_3$/NMAc, LITFSI/NMAc, and $LiPF_6$/NMAc DES systems. Reproduced with permission. Copyright 2013, Royal Society of Chemistry c) Conductivity and viscosity of $Zn(TFSI)_2$/Ace DESs at different molar ratios, and d) comparison of linear sweep voltammetry of different DESs. The scanning rate is 1 mV $s^{-1}$, and the working electrode is stainless steel. Reproduced with permission. [31] Copyright 2019, Nature Publishing Group.

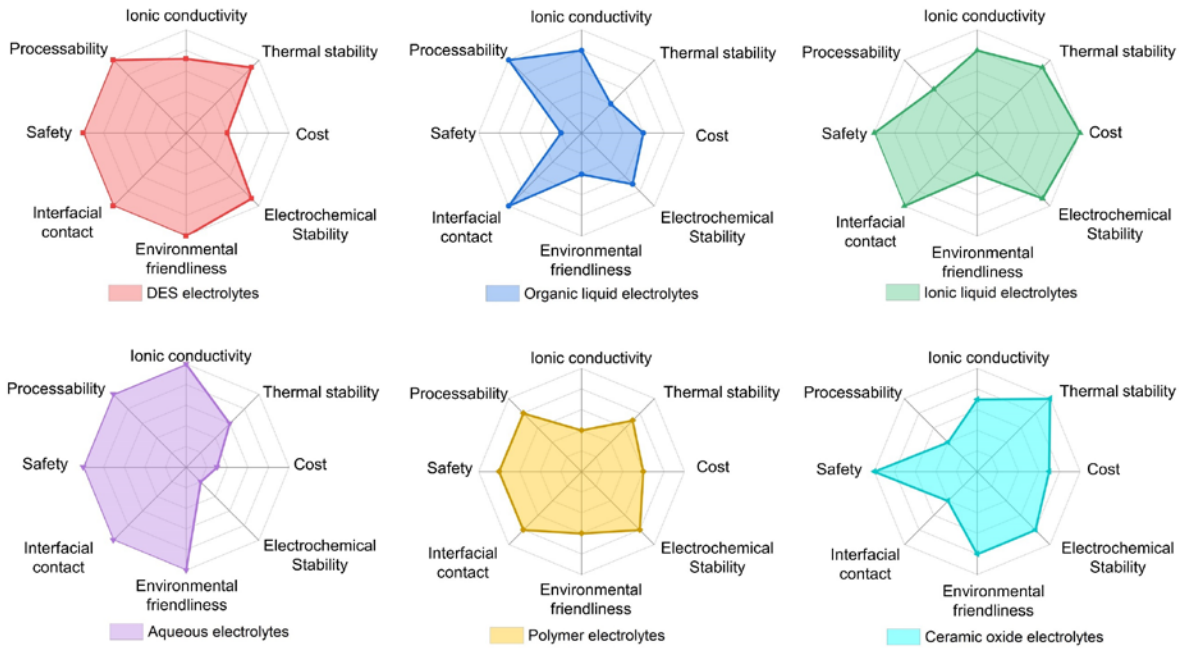


**Figure 3.** Radar plots of the properties of different types of electrolytes. The values (distances from the center) range from 0 to 5, where 5 corresponds to the highest value of a certain property. 0 means certain properties do not apply to this type of electrolyte.

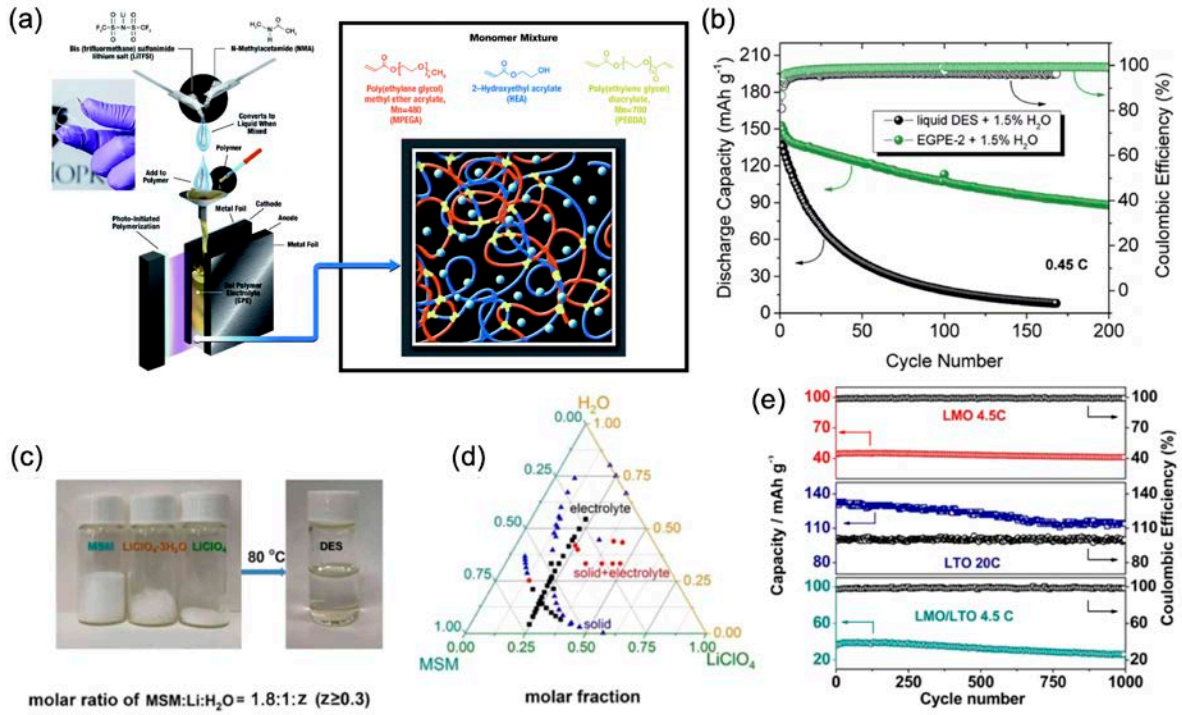


**Figure 4.** a) Schematic illustration showing the fabricating process of UV-cured DES-based GPEs. b) Comparison of cyclic performance of LMO||LTO full cells with DES-based GPEs and liquid DES. Reproduced with permission [48]. Copyright 2020, Royal Society of Chemistry. c) Stoichiometric amounts of MSM, $LiClO_4$, and $LiClO_4 \cdot 3H_2O$ are used to prepare a room-temperature DES-0.3 (MSM:$LiClO_4$:$H_2O$ = 1.8:1:0.3). d) State of m$MSM$–n$LiClO_4$–z$H_2O$ salt–water mixtures, where m, n, and z are the molar ratios for MSM, $LiClO_4$, and $H_2O$, respectively. The stable liquid state, solid phase, and partially miscible phase are drawn by black squares, blue triangles, and red circles, respectively. e) Cycling performance of the LMO cathode at a rate of 4.5 C, LTO anode at a rate of 20 C, and LMO||DES-1||LTO battery at a rate of 4.5 C, respectively. Reproduced with permission [50]. Copyright 2019, American Chemical Society.

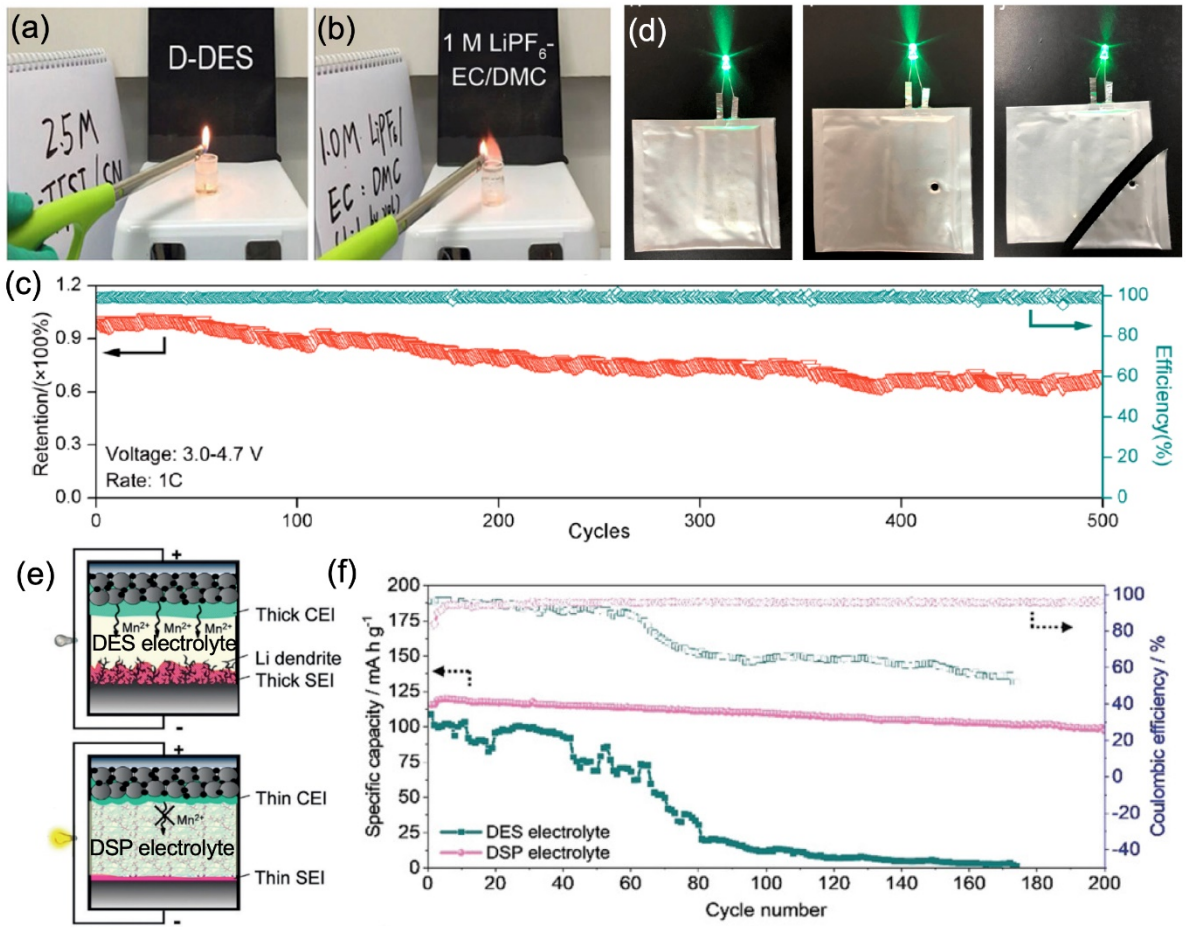


**Figure 5.** Flammability test of a) SN-based DES and b) 1 M $LiPF_6$-EC/DMC electrolytes on a heating plate at 200 °C. c) The capacity retention of $LiCoO_2$||Li half-cells cycled in the SN-based DES electrolyte at a rate of 1 C within the voltage between 3.0 and 4.7 V. d) Optical images showing the stability of $LiCoO_2$||Li pouch cells with SN-based DES electrolyte before and after the nail and cut tests. Reproduced with permission [55]. Copyright 2020, American Chemical Society. e) Schematic illustration showing the benefits of using DSP electrolyte in Li||LMO. f) Cyclic performance at 0.1 C of Li||DES electrolyte||LMO and Li||DSP electrolyte||LMO cells. Reproduced with permission [56]. Copyright 2020, John Wiley and Sons

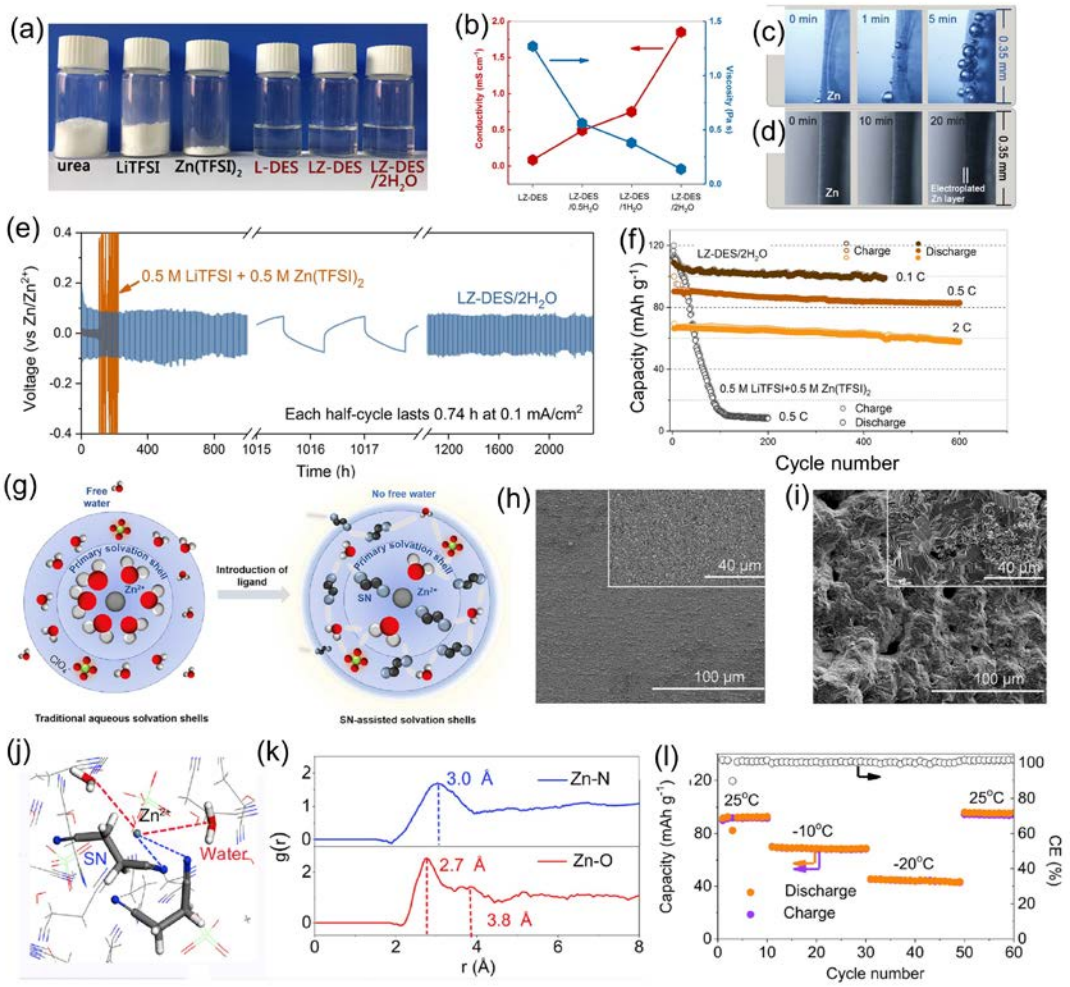


**Figure 6.** a) Stoichiometric amounts of urea, LiTFSI, and $Zn(TFSI)_2$ used to prepare different (DESs L-DES, LZ-DES, and LZ-DES/$2H_2O$). b) Conductivity and viscosity of DESs with different water ratios. In situ optical microscopic images of the Zn electrodeposition process in c) 0.5 M LiTFSI + 0.5 M $Zn(TFSI)_2$ and d) LZ-DES/$2H_2O$ at 0.2 mA $cm^{-2}$. e) Voltage profiles in a Zn||Zn symmetrical cell at 0.1 mA/$cm^2$ (each half-cycle lasting for 0.74 h). f) Cycling performance of the Zn||LMO cell in LZ-DES/$2H_2O$ under various rates, in comparison with those in 0.5 M LiTFSI + 0.5 M $Zn(TFSI)_2$. Reproduced with permission [32]. Copyright 2019, Elsevier. g) Schematic diagrams of $Zn^{2+}$ solvation structures in aqueous and SN-based ZS electrolytes. h and i) SEM images of Zn metal plated on the stainless-steel collector in ZS and ZW electrolytes, respectively. j) A snapshot obtained by MD simulations and representative

$Zn^{2+}$ solvation structure in the ZS electrolyte. k) RDFs for $Zn^{2+}$–N and $Zn^{2+}$–O. l) Electrochemical performance of the PDB||ZS||Zn battery at room temperature and low temperature. Reproduced with permission [67]. Copyright 2020, Elsevier.

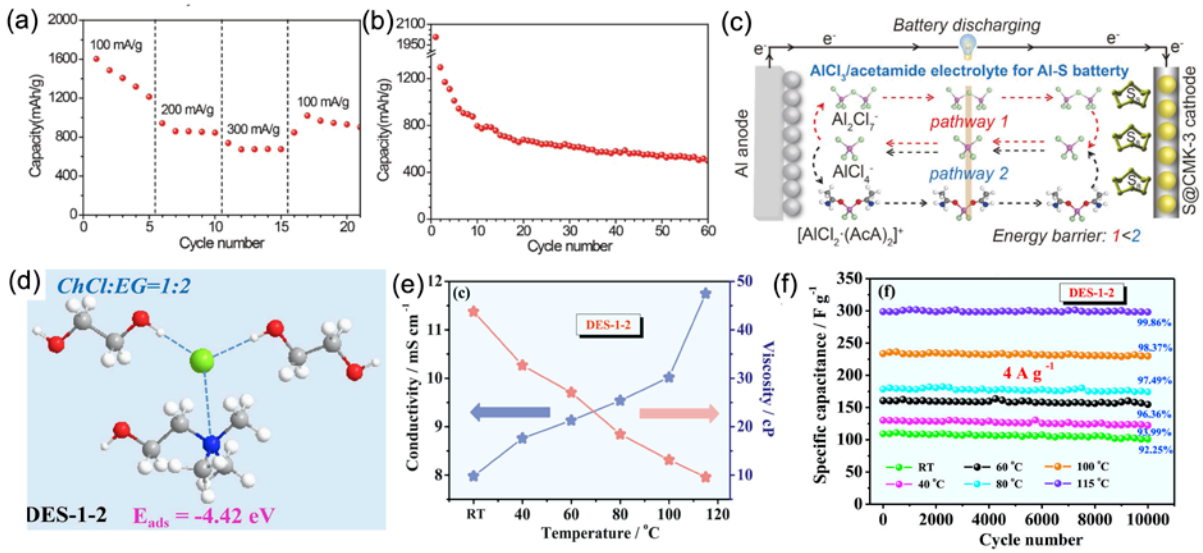


**Figure 7.** a) Rate performance and b) cyclic stability of Al–S battery using $AlCl_3$/Ace DES. c) Schematic illustration of the battery discharging process for Al–S battery. Reproduced with permission [73]. Copyright 2019, Elsevier. d) Structure of DES-1-2 based on DFT calculation. e) The viscosity and electrical conductivity of DES-1-2 samples at different temperatures from RT to 115 °C. f) Cyclic performance of the activated carbon-based supercapacitor using DES-1-2 as electrolyte at different temperatures from RT to 115 °C. Reproduced with permission [87]. Copyright 2020, Elsevier.

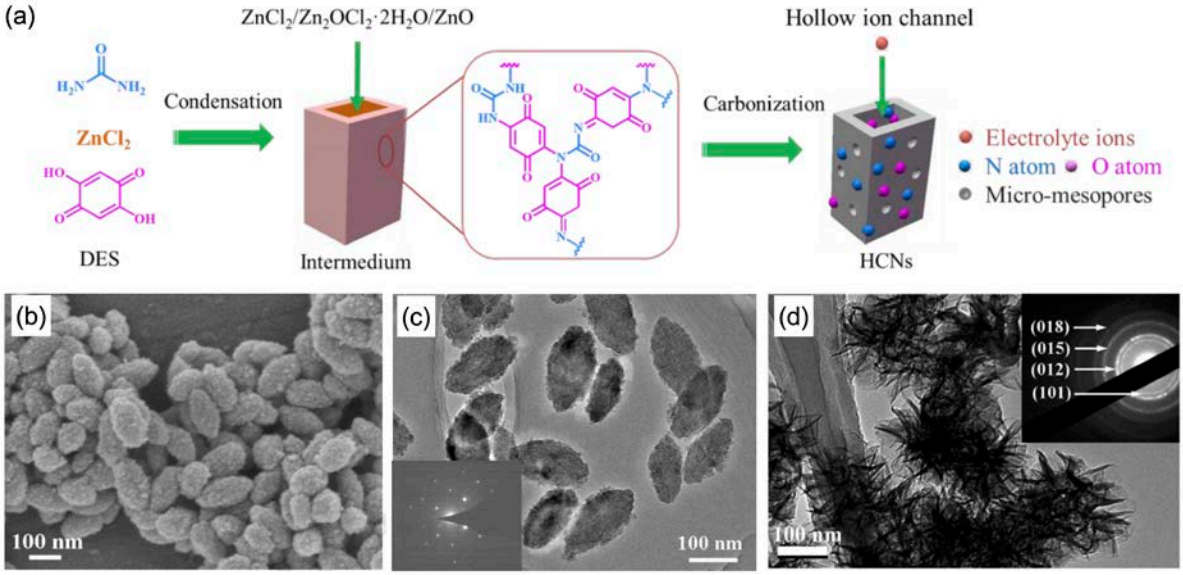


**Figure 8.** a) Schematic illustration showing the fabrication process of HCNs. Reproduced with permission.[104] Copyright 2019, Royal Society of Chemistry. b) SEM and c) TEM images of $Fe_2O_3$ nanospindles. The inset of (c) shows the corresponding SAED pattern. Reproduced with permission [35]. Copyright 2015, Elsevier. d) TEM image and SAED pattern of nanoflower-like $\alpha$-$Ni(OH)_2$. Reproduced with permission [108]. Copyright 2013, Royal Society of Chemistry.

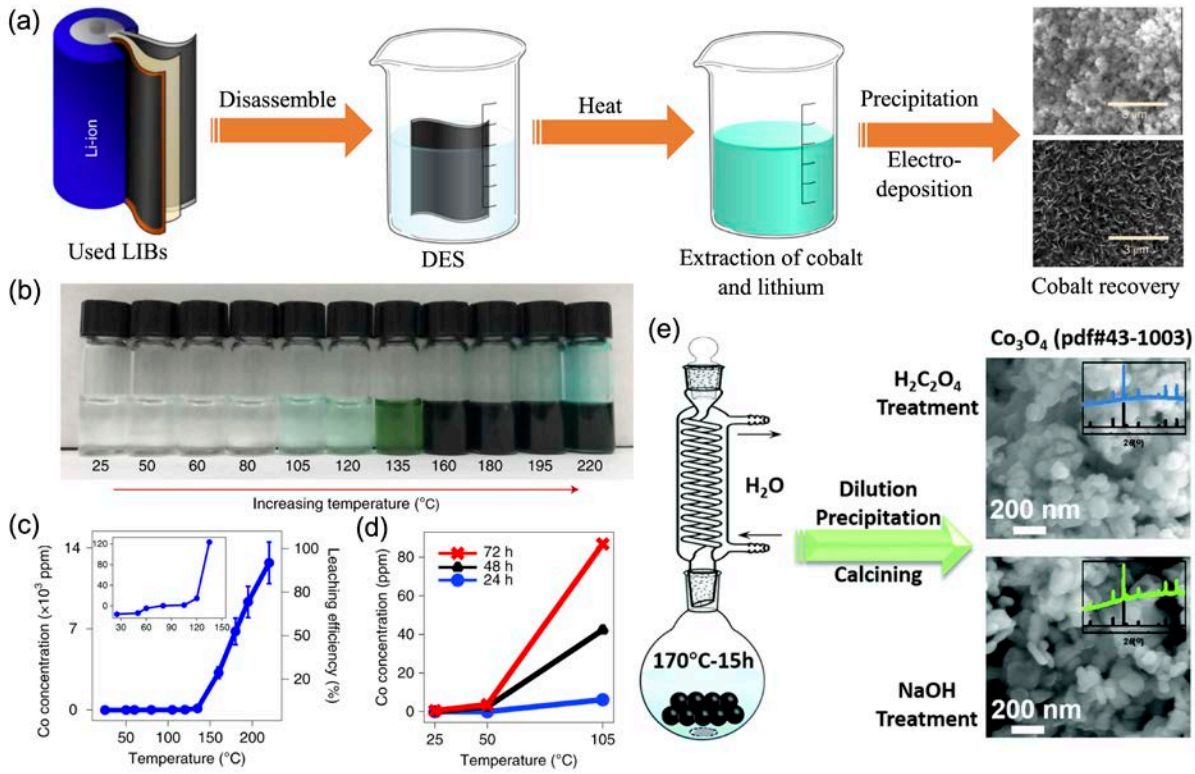


**Figure 9.** a) Schematic of the battery recycling process using a DES. b) Photograph of the color change when $LiCoO_2$ is dissolved to DES (which is clear in its pure form) at different temperatures. c) Co concentration and leaching efficiency at different temperatures with a fixed time of 24h. d) Co concentration versus temperature with different reaction times (24h, 48h, and 72h). Reproduced with permission [120]. Copyright 2019, Nature Publishing Group. e) Recycling of spent LIBs using ChCl/urea DES and the following treatments. Reproduced with permission [121]. Copyright 2020, Royal Society of Chemistry.

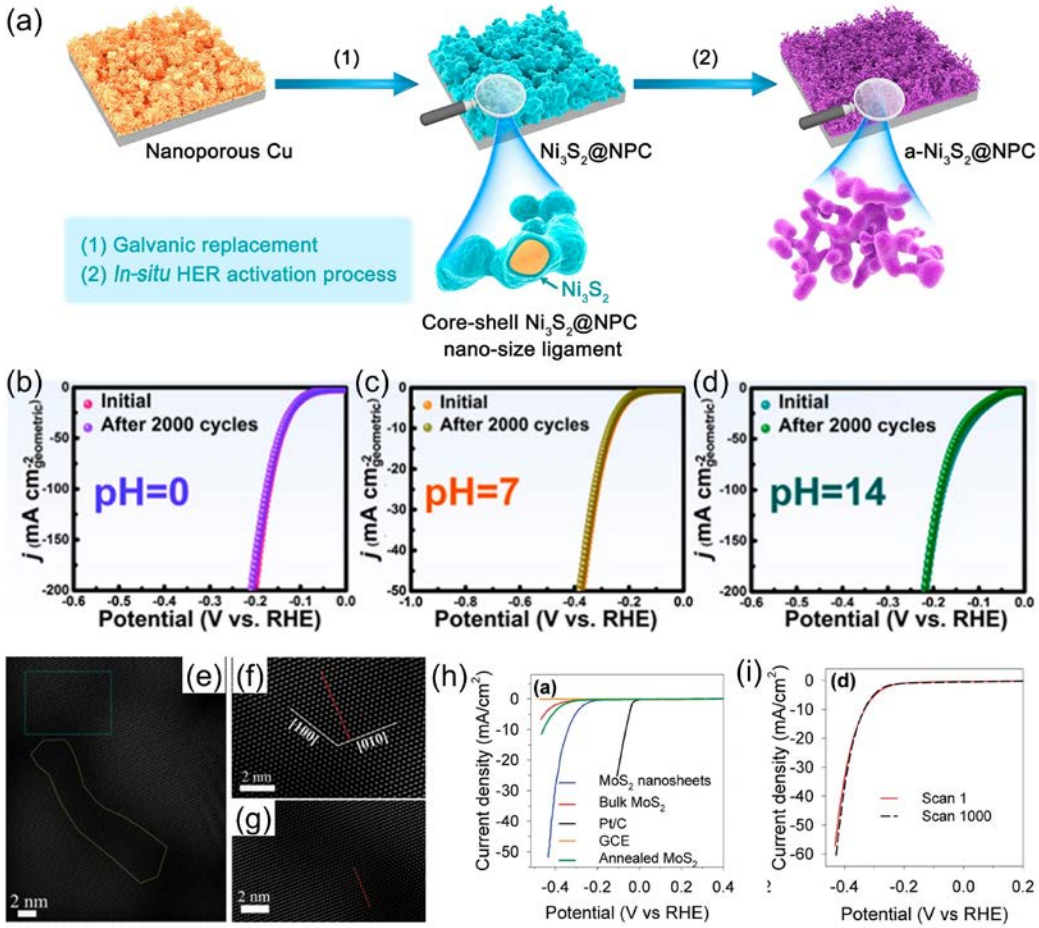


**Figure 10.** a) Schematic illustration showing the fabrication process of the nanoporous $Ni_3S_2$@NPC electrode and the in-situ activation process during HER electrolysis. b-d) Polarization curves of a-$Ni_3S_2$@NPC in acidic (pH=0), neutral (pH=7), and alkaline (pH=14) solutions before and after 2000 cycles. Reproduced with permission [33]. Copyright 2017, Elsevier. e) HRTEM image of the $MoS_2$ nanosheets after applying fast Fourier transform (FFT). The regions enclosed by blue and yellow lines are 1T and 2H phases of $MoS_2$, respectively. Higher magnifications of the f) 1T- and g) 2H-$MoS_2$ within a single nanosheet. h) Polarization curves of the exfoliated and bulk $MoS_2$ as well as Pt/C with the scan rate of 2 mV/s. i) Stability test of the $MoS_2$ nanosheets in 0.5 M $H_2SO_4$. Reproduced with permission [114]. Copyright 2018, American Chemical Society.

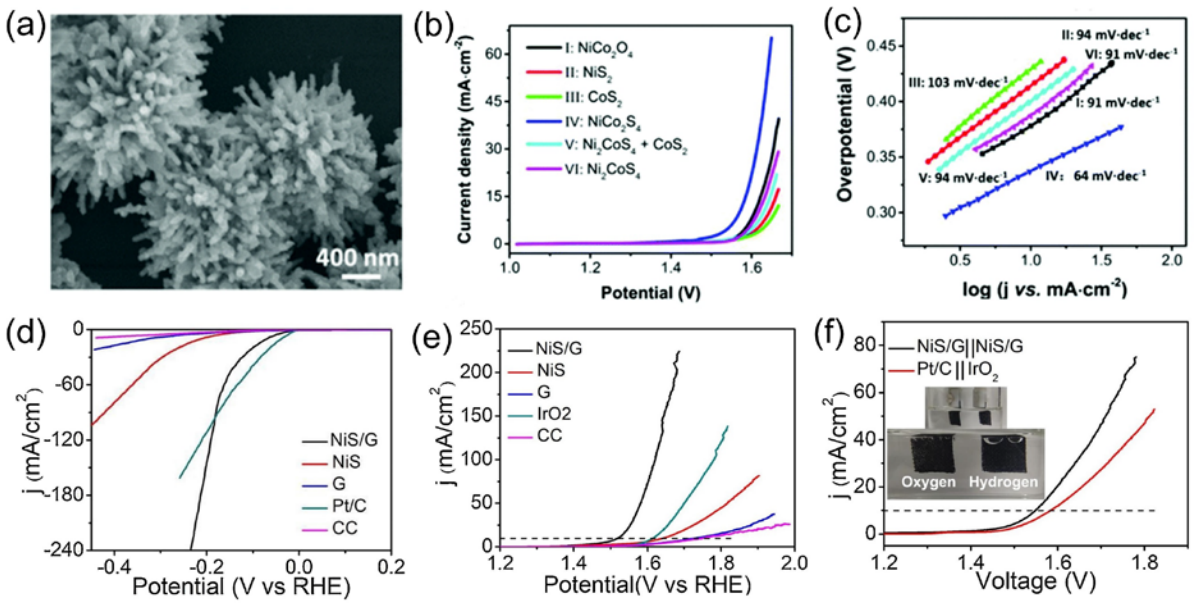


**Figure 11.** a) SEM images of the sea urchin-like $NiCo_2S_4$; b) polarization curves of $NiCo_2O_4$, $NiS_2$, $CoS_2$, $NiCo_2S_4$, $Ni_2CoS_4$ + $CoS_2$, and $Ni_2CoS_4$ modified GC electrodes in 1 M KOH at 5 mV $s^{-1}$ utilizing an Ag/AgCl (3 M KCl) electrode and Pt wire as the reference and counter electrode, respectively; c) Tafel plots obtained from polarization curves in (a). Reproduced with permission [134]. Copyright 2017, Royal Society of Chemistry. d) HER LSV curves of NiS/G, NiS, G, 20% Pt/C, and bare CC electrodes; e) OER LSV curves of NiS/G, NiS, G, and $IrO_2$ on CC and bare CC electrodes. f) LSV curves of NiS/G-3 as HER and OER bifunctional catalyst for overall water splitting (the inset is a digital photograph of the two-electrode cell), Pt/C and $IrO_2$ were measured for comparison. Reproduced with permission [136]. Copyright 2019, Elsevier.

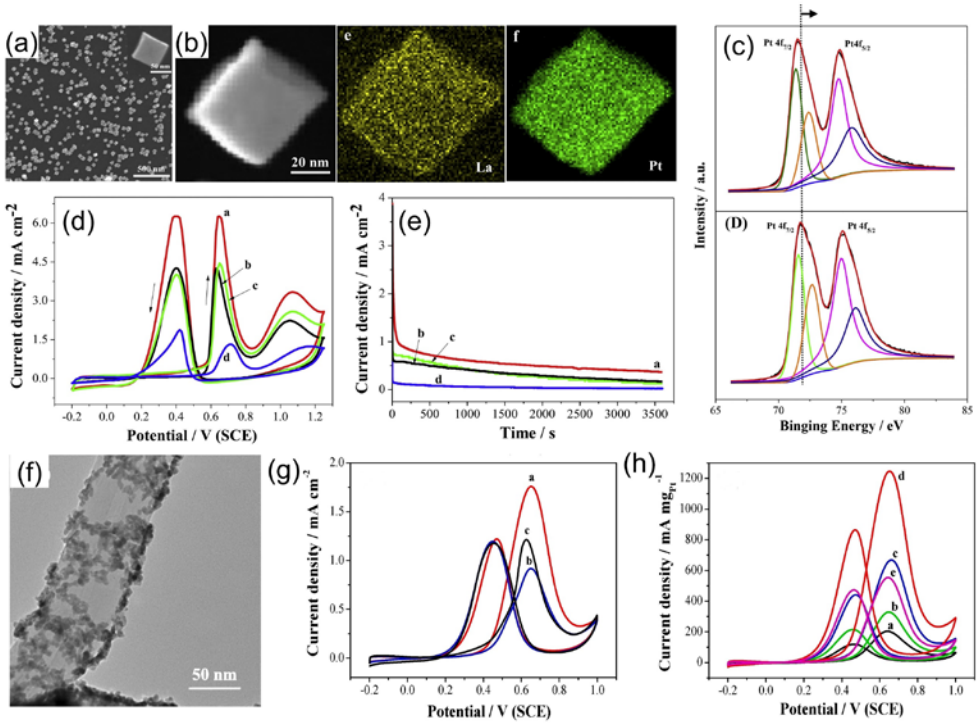


**Figure 12.** a) SEM image of concave cubic PtLa alloy NCs. The inset of (a) is the high-magnification SEM image of a single PtLa alloy NC particle. b) STEM and EDX elemental maps of PtLa alloy NC particle. c) Pt 4f spectra of pure Pt NCs (top) and PtLa alloy NCs (bottom). d) CV curves (50 mV $s^{-1}$) and e) CA curves recorded at 0.6 V of ethanol oxidation on (a) $Pt_{10}La_5$ , (b) $Pt_{10}La_1$, (c) pure Pt, and (d) $Pt_{10}La_{10}$ NCs in 0.5 M ethanol + 0.5 M $H_2SO_4$ solution. Reproduced with permission. [36] Copyright 2018, Elsevier. f) TEM image of $Pt_1Cu_{0.25}$ ANCs/MWCNTs. g) CV curves (50 mV $s^{-1}$) of (a) $Pt_1Cu_{0.25}$ ANCs/MWCNTs , (b) Pt/MWCNTs-D , and (c) Pt/MWCNTs-W in the same solution. h) CV curves (50 mV $s^{-1}$) of PtCu ANCs/MWCNT catalysts prepared with different Pt:Cu mass ratios of (a) 1:1, (b) 1:0.67, (c) 1:0.43, (d) 1:0.25 and (e) 1:0.11 in a 0.5 M $H_2SO_4$ solution containing 0.5 M $CH_3OH$. Reproduced with permission.[143] Copyright 2019, Elsevier.

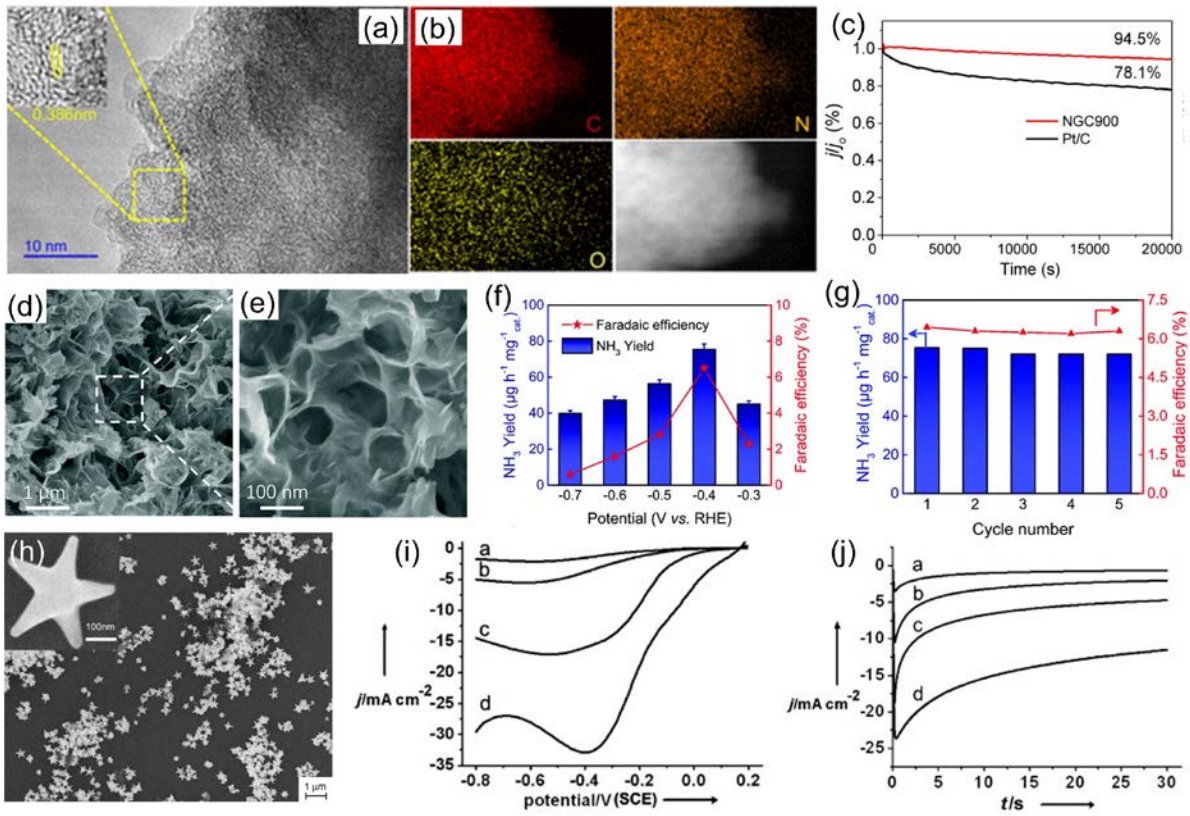


**Figure 13.** a) HRTEM images and b) EDS elemental mapping of NGC900. c) Current–time (*I*–*t*) test of NGC900 and Pt/C (relative decrease in the current) at the rotation rate of 1600 rpm in an $O_2$-saturated 0.1 M KOH aqueous solution. Reproduced with permission.[154] Copyright 2017, American Chemical Society. d,e) SEM images of $Fe_3S_4$ nanosheets; f) yield of $NH_3$ and faradaic efficiency at each given potential; g) cycling test of the NRR for $Fe_3S_4$ nanosheets. Reproduced with permission [159]. Copyright 2018, Royal Society of Chemistry. h) SEM images of the star-shaped Au NPs. i) Current–potential curves of electrocatalytic reduction of 20 mM $H_2O_2$ in 0.1 M phosphate-buffered solution at a scan rate 50 mV $s^{-1}$ and j) transient current-density curves of 20 mM $H_2O_2$ reduction at −0.5 V; (a) polycrystalline Au electrode, (b) snowflake-like Au NPs, (c) nanothorns, and (d) star-shaped Au NPs. Reproduced with permission [161]. Copyright 2008, John Wiley and Sons.

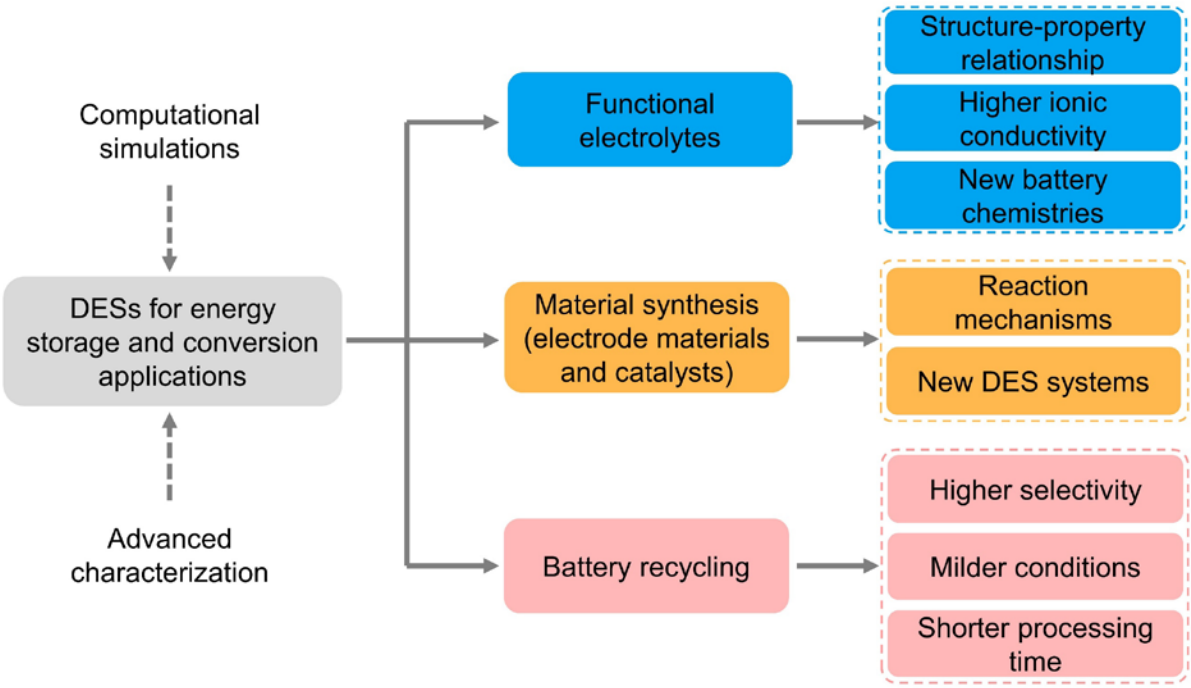


**Figure 14.** The future research directions on DESs in energy storage and conversion applications.

**Table 1.** Freezing temperature, viscosity, and ionic conductivity of various DESs.

| Salt | HBD | Salt:HBD (molar ratio) | Freezing temperature (at DES point, $T_f$ (℃)) | Viscosity (mPa·s, at 25 ℃) | Ionic Conductivity (mS $cm^{-1}$, at 25 ℃) | Ref |
|---|---|---|---|---|---|---|
| ChCl | urea | 1:2 | 12 | 750 | — | [25] |
| ChCl | acetamide | 1:2 | 51 | — | — | [25] |
| ChCl | ethylene glycol | 1:2 | −66 | 37 | 7.61 at 20 ℃ | [165] |
| $ZnCl_2$ | urea | 1:3.5 | 9 | 11340 | — | [166] |
| $ZnCl_2$ | acetamide | 1:4 | −16 | — | — | |
| $ZnCl_2$ | ethylene glycol | 1:4 | −30 | — | — | |
| LiTFSI | N-methylacetamide | 1:4 | −72 | 78.38 | 1.35 | [26] |
| $LiNO_3$ | N-methylacetamide | 1:4 | −75 | 107.19 | 0.76 | |
| $LiPF_6$ | N-methylacetamide | 1:4 | −52 | — | 1.41 | |
| LiTFSI | urea | 1:3.6 | −37.60 | — | 0.23 | [45] |
| LiTFSI | acetamide | 1:4 | −67 | 99.56 | 1.07 | [27] |
| LiBETI | acetamide | 1:4 | −57 | 222.4 | ~0.8 | [167] |
| $Zn(TFSI)_2$ | acetamide | 1:4 | −35.70 | 2130 | 0.16 | [31] |
| | | 1:5 | −36.20 | 1890 | 0.19 | |
| | | 1:7 | −51.32 | 789 | 0.31 | |
| | | 1:9 | −51.51 | 533 | 0.51 | |
| $Zn(ClO_4)_2·6H_2O$ | succinonitrile | 1:4 | −91 | ~45 | ~0.8 | [67] |
| | | 1:6 | −89.4 | ~33 | ~2.3 | |
| | | 1:8 | −95.3 | 25.4 | 5.52 | |